People's Democratic Republic of Algeria
Ministry of Higher Education and Scientific Research

University M'Hamed BOUGARA – Boumerdes

Institute of Electrical and Electronic Engineering

Department of Power and Control Engineering

Final Year Project Report Presented in Partial Fulfilment of
the Requirements for the Degree of

MASTER

In **Electrical and Electronic Engineering**

Option: **Power and Control Engineering**

Title:

Maximum power point tracking of Solar pumping system based on BLDC motor under partial shading condition

Presented by:

- **Belguellaoui Moufida (Control option)**
- **Hamraoui Kahina (Power option)**

Supervisor:

Dr. Ammar Abdelkarim

Registration Number: ……../2021

Abstract

This thesis is part of the research work dedicated for exploitation of solar photovoltaic energy. Due to the increasing energy demands, the use of photovoltaic energy has increased significantly in the worldwide, especially in remote and isolation regions. Off-grid photovoltaic systems, particularly water pumping system, is becoming more widespread. The use of photovoltaic energy as an energy source for water pumping is considered as one of the most promising areas of the photovoltaic applications. The photovoltaic pumping systems are basically operated in two ways, with or without battery bank. The study presented in this thesis focuses on the improvement of photovoltaic power extracting for a battery-less pumping system. In this context, many researchers are committed to invent the algorithms for extracting the maximum energy from a photovoltaic array. It is the principle named maximum power point tracking (MPPT), which is the main object of our research. In the first, an MPPT strategy based on the cuckoo swarm optimization technique has been developed to improve the performance of the perturb and observe (P&O) algorithm under sudden irradiance changes and partial shading condition. Afterwards, a high-performance control scheme has been developed for a photovoltaic pumping system based on the brushless DC motor, in order to maximize the delivered power by the photovoltaic array, to maintain the speed of the motor and to regulate the DC-link voltage. The control scheme is based on hysteresis control. In addition, this scheme has been confirmed through simulation performed with MATLAB/Simulink.

Keywords: Photovoltaic (PV), Maximum power point tracking (MPPT), Partial shading, Brushless Direct current motor (BLDC), Pump.

Dedication

To my lovely parents, to my dear brother, to my sweet sisters, to my nephews and to every member of my family for keeping me forward even when it seemed hard and impossible, for their love, support and encouragement.

To my best friends Wissem, Sarah and Hidayet for being there for me during the hardest days of university and making them better.

To my best friend and partner Kahina who encouraged me always since the day I met her.

Thank you

Moufida

To my lovely parents Said and Bahia, they are both responsible for the good values that guide my life.

To my dear brother Yanis, To my sweet sister Sabrina.

Thank you

Kahina

Acknowledgement

In the name of ALLAH, the Most Gracious and the Most Merciful. Thanks to ALLAH who is the source of all the knowledge in this world, for the strengths and guidance in completing this thesis.

We express our deep sense of gratitude and heart-felt thanks to our supervisor, Dr AMMAR Abdelkarim, for his invaluable guidance, patience, kindness and consistent encouragement throughout the course of this work. We cannot forget to mention all our friends for their great friendship, help and support.

We take this opportunity to record our sincere thanks to all INELEC teachers, stuff and our colleagues for their valuable help.

Kahina and Moufida

List of content

LIST OF TABLES

LIST OF FIGURES

List of abbreviations:

PV Photovoltaic

P Power [w]

V Voltage [V]

I Current [A]

PI Proportional-Integrator

MPP Maximum Power Point

MPPT Maximum Power Point Tracking

STC Standard Test Conditions [25°C, 1sun]

G Irradiance [W/m2]

$P\&O$ Perturb and Observe

PSO Particle Swarm Optimization

CS Cuckoo Search

$Pmax$ Maximum Power

DC Direct Current

AC Alternating Current

PWM Pulse Width Modulation

SWPS Solar Water Pumping System

PVG Photovoltaic Generator

PVS Photovoltaic System

GW Gigawatt

I-V Current-Voltage

VSI Voltage Source Inverter

UNDP The United Nations Development Program

CO2 Carbon Dioxide

BLDC Brushless DC

PMBLDC Permanent Magnet Brushless DC

Si Silicon

Ish Short Circuit Current

Voc Open Circuit Voltage

MOSFET Metal Oxide Semiconductor Field Effect Transistor

IGBT Insulated Gate Bipolar Transistor

ECM Electronic Commutation Motor

EMF Electromotive Force

BEMF Back Electromotive Force

List of symbols:

I_{PV} Photovoltaic current

V_{PV} Photovoltaic voltage

I_O Saturation current [A]

V_{mp} Maximum power point voltage

I_{mp} Maximum power point current

V_{OC} Open circuit voltage

I_{sc} Short circuit current

N_S Number of series connected cells

K_P Proportional constant

K_I Integrator constant

I_{ph} photocurrent

I_d junction diode current

I_0 reverse saturation current

R_s series resistance

R_{sh} parallel resistance

A diode factor

k Boltzmann's constant

T Cell temperature

Eg gap energy (1.12 eV for Crystalline-Silicon)

q electron charge

T_{ref} reference temperature of PV cell in Kelvin (K), usually 298K (250C)

η efficiency of the module

FF the fill factor

M index to the module

n_s number of cells connected in series

n_p number of cells connected in parallel

R_{sM} Series resistance of module.

I_{srM} is the reference saturation current of Module

I_{ccrM} the reference short circuit of module

I_{scM} The short circuit of the array under given environmental conditions

D The duty cycle.

L The value of inductor

C capacitor

a,b,c Indices denoting actual three phase axes

P Number of pair poles

Te Electromagnetic toque

TL Load torque

V_{aN}, $V_{bN,}$ V_{cN} Phase-to-neutral voltages of the inverter (V)

V_{DC} DC-link voltage (V)

Q Flow rate (liter/s or m^3/s)

R Boost resistive load (Ω)

General introduction

Solar energy is a more familiar source of renewable energy because of several advantages. Photovoltaic (PV) power systems have been widely used in many countries and research. However, there are many problems in handling the applications of PV power systems because the unstable behavior related mainly to irradiance. Among the main applications of PV systems are either standalone (water pumping, street lighting, electric vehicles, military and space applications) or grid-connected configuration (power plants, hybrid systems). Today these applications cover only 0.5% of world energy consumption but solar energy will be one of the most important renewable energy sources in the future.

Among all other application based solar PV system, water pumping is most effective, crucial and cost-effective application for power generation by Solar PV array. The stand-alone photovoltaic (PV) water pumping system has received increasing attention in the last 20 years because of the significant, on-going cost reductions achieved in manufacturing PV arrays [1].

Unfortunately, The tracking of the correct maximum power point is essential in PV systems to ensure the best energy harvesting from the environment conditions. Moreover, the available output power of PV array fluctuates with change in ambient temperature and solar irradiation[1].Therefore, maximum benefits from solar PV, is obtained by using Maximum Power Point Tracking (MPPT) algorithm. Many studies were made on MPPT methods and developed for either stand-alone or gridconnected PV systems which were installed in wide-ranging power capacities and by using various technologies[2].

One big issue that influences the performance of PV system is the partial shading condition. Under this condition, the PV power versus voltage curve includes many points of maximum power so any conventional MPPT is unable to identify the global peak[1]. Motivated by the above concerns, this thesis focuses on the formulation of MPPT algorithms that are simple and robust to the atmospheric condition changes. Several global tracking techniques based on modern optimization are proposed in order to extract the global MPP under shading condition. These techniques include Cuckoo Search and Particle Swarm Optimization which this thesis focuses on. The aim of this thesis is to establish a reliable system able to operate efficiently under sudden variable conditions like irradiation, voltage, power. Moreover, to ensure a smooth start and operation of the BLDC motor.

To better match the PV array to the motor-pump set, a pump controller is required. Generally, a boost converter is used to operate system at higher voltage level. The use of

BLDC motor for both pumping system technique along with solar PV source increases its utilization and reliability. The parameters of the brushless direct current motor are controlled by using hysteresis control through gate driver circuit of the VSI. The project is designed such that it operates under variable conditions like changes of irradiation, voltage, power.

- **Thesis organization:**

The research presented in this thesis is organized into four chapters. The work carried out in each chapter is summarized as follows:

- Chapter-1: This chapter gives a background and a general overview on photovoltaics and solar water pumping systems. These systems were also classified based on the energy storage, the electric power input and type of pump. A brief description of the used SWPS was presented by the end.
- Chapter-2: This chapter describes the components models of an off-grid photovoltaic system for water pumping. These models are used in the following chapters for control design and simulation work.
- Chapter-3: In this chapter, a review of the most widely used maximum power point algorithm for photovoltaic systems is presented. Furthermore, a short overview of the control of the BLDC motor is described in this chapter.
- Chapter-4: The proposed algorithms are employed with hysteresis current controller. Simulation results are provided to demonstrate the validity and the performance improvement of the proposed algorithms.

Chapter 1

Introduction

1.1 Introduction

Water resources are essential for satisfying human needs, ensuring food production and protecting health, as well as for social and economic development. Water pumping worldwide is generally dependent on electricity or diesel generated electricity. The diesel is expensive and not available in countryside of many developing countries and even when the fuel is available, transporting it to remote areas is not an easy task. This is because there are no roads or supporting infrastructure in most of the remote villages [1]. The electricity must be economic and takes minimum maintenance when this power is available from the nearby grid. In rural areas, the installation of a new transmission line and transformers is extremely expensive for irrigation or drinking water [2].

Photovoltaic energy offers an excellent solution for providing sustainable and clean energy to remote and rural areas. Over the past decade, several major advances have been made in solar cells design, and large-scale manufacturing techniques, as well as new developments in system component technology. These, in turn, have resulted in a dramatic cost reduction for solar applications. This cost reduction has made solar generation rivals established fuel technologies as a cleaner, more economical choice.

Other than being economically competitive, solar water pumping systems are more reliable and require less maintenance. Due to these benefits, solar water pumping for irrigation, livestock, and domestic use has become the most common PV application and is now widely deployed not only for small farms/ranches but also for large-scale irrigation schemes. With

countries even announcing ambitious targets for solar pump installations over the next decade [3][4]. In this chapter, a theoretical review is presented about of the photovoltaic system and the solar water pumping system.

1.2 Introduction to Photovoltaic

Demand for energy and associated services, to meet social and economic development and improve human welfare and health, is increasing. Global use of fossil fuels (coal, oil and gas) has increased to dominate energy supply, leading to a rapid growth in carbon dioxide (CO2) emissions.

The solar energy appears to be the most promising to overcome these global problems. The solar energy is much greater than all other renewable and fossil-fuel-based energy resources combined where the sunlight that reaches the earth's surface is almost 6000 times the average power consumed by humans [5]. Solar photovoltaic systems (PV) have achieved grid parity in many countries, and several targets have been set to achieve 100 per cent renewable energy systems by 2050. Moreover, it is expected that the cost of renewables will likely undercut fossil fuels in the next 10 years [6]. In 2019 the solar PV market increased an estimated 12% to around 115 GW [7]. The annual and cumulative installed PV power capacity worldwide is shown in Figure 1.1:

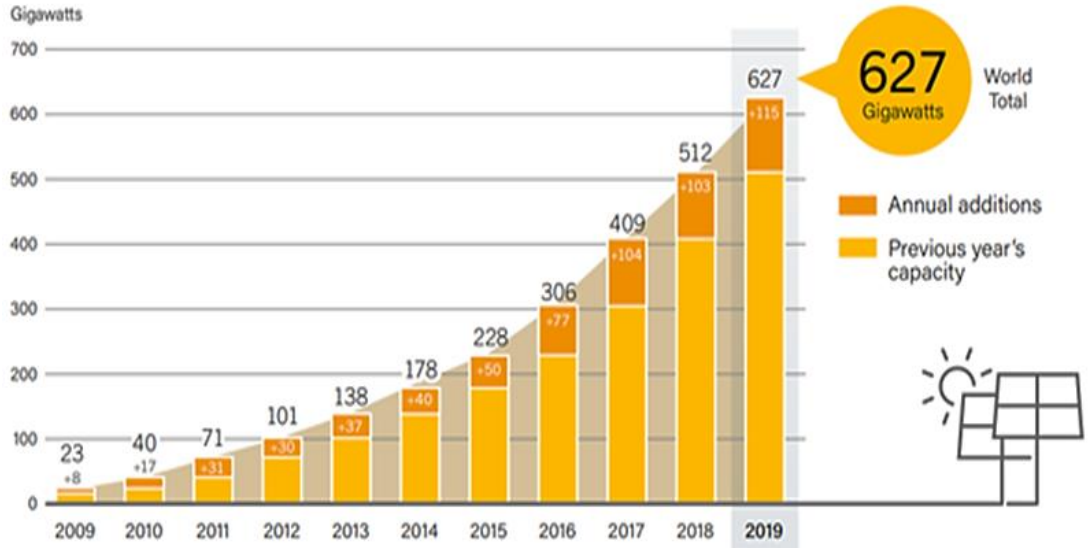

Figure 1.1: Global annual and cumulative installed PV power from 2006 to 2019.

The key reason for this significant development is the increased competitiveness of PV energy because of the cost reduction of PV modules and the introduction of economic incentives

or subsidies. This has made PV-generated electrical energy cost-effective and competitive in some regions of the world with good solar irradiation conditions. In addition, PV systems can range from small scale to large scale, making it possible to implement PV systems by individuals compared to other renewable energy sources (wind, marine, geothermal, etc.) that have higher capital costs [8].

PV systems are widely operated in grid-connected and a stand-alone mode of operations. Grid-connected PV energy conversion systems are designed to be able to inject a sinusoidal current into the utility grid. These systems can be grouped into two classes of applications: distributed generation or centralized power systems. Distributed generation systems are installed to deliver power to a grid-connected customer or directly to the grid. On the other hand, centralized PV power systems offer bulk power in order to reduce fuel sources dependency and greenhouse gases. In the grid-connected condition when solar radiation is insufficient and unable to meet load demand, the energy is accessed from grid via net meter which makes more reliability in the consumer ends.

Off-grid solar PV system is independent of the grid and provides freedom from power quality issues and electricity billing. The excess energy can be accumulated in the battery storage units through superior control [9]. These systems consist of several components that convert solar energy into electrical energy in a controlled, reliable and efficient manner to provide DC or AC loads. Off-grid photovoltaic power generation system is one of the best choices to meet the electricity demand in remote areas or remote areas (mains unavailable or expensive). Among the many applications of off-grid photovoltaic systems, the pumping system is one of the most promising and attractive systems in various fields such as household and livestock water supply, small irrigation systems, and fish farms [8].

1.3 Background of Solar Water Pumping System

1.3.1 Historical review

Solar water pumping system has been a promising area of research for more than 50 years. In the early 70s, efforts and studies were undertaken to explore the possibility of solar pumping system as feasible, viable and economical mean of water pumping.

The history of efforts made to convert solar energy into mechanical energy / electrical energy to pump water dates back to around 15th–19th century. The first case of solar PV water

pump reported in 1964 in the Soviet Union. However, the flowrate and working head of the water-pumping systems were small, but these studies finally proved milestones in the development of future solar operated water pumping system. The first large scale PV operated pumping system was constructed on an experimental basis in 1977 in Mead, Nebraska. The water pumping capacity of this system was 3.8 m^3per minute and could run for 12hours a day[10].

Besides, Within the framework of a solar pumping project in the early 1980's, The World Bank and The United Nations Development Program (UNDP) assessed these first pumps and encountered several cases of incorrect wiring, failure of electronic circuitry, dangerous DC voltages and terminals that did not provide good electrical connection. Probably the most significant challenge was a financial one: solar technology was very expensive in this period, which made it unaffordable for farmers. Since 2009, solar panels started to become increasingly affordable due to the decrease in price, and technical improvements have resulted in increasing use of solar pumps [11].

1.3.2 Classification of Solar Water Pumping System

1.3.2.1 Based on the energy storage

This classification of SWPS is based on, whether the electricity generated is stored in the battery/battery bank or directly utilized to drive the pump. On this basis, SPVWPS is further classified and described as follows:

- **Battery-coupled**

Battery-coupled SWPS as shown in Figure 1.2 consists of a solar panel, charge controller, batteries, pump controller, pressure switch, storage tank and a DC water pump. During the day-time, the solar panels convert the solar energy into electrical current that charges the batteries. These batteries, then supply power to pump for pumping the water when needed. These charged batteries in SWPS can prolong the water pumping duration. The use of the batteries in SWPS ensures water pumping even during low light periods, cloudy days and during the nights. However, its use increases the cost, complexity and can reduce the overall efficiency of the system as the batteries dictate the operating voltage rather than the PV panels [10].

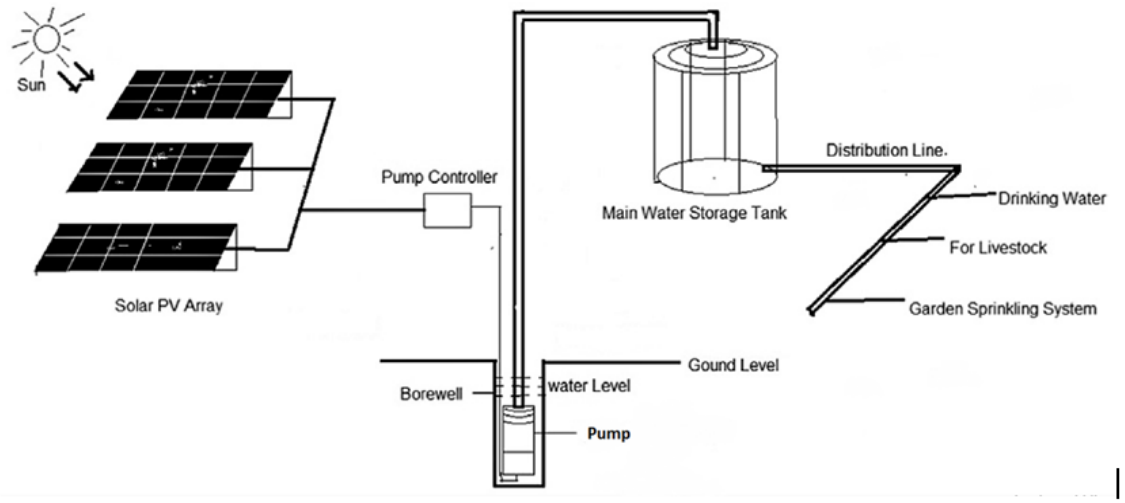

Figure 1.2: Battery coupled solar PV water pumping system.

- **Direct driven**

Direct driven solar PV water pumping system is shown in figure 1.3. In this system, electricity generated by PV modules is directly supplied to the pump. The pump uses this electric power to pump the water. As no backup power is available, the system pumps water during the daytime only when the solar energy is available. The intensity of the solar irradiation incident on the solar panel decides the amount of water pumped during that time. The advantage of this system is that, it is battery free, simple and low in cost as compared to battery coupled SWPS. However, it cannot be used to pump water during the night [10]. Also, because of Partial shading effect the amount of water pumped also changes throughout the day.

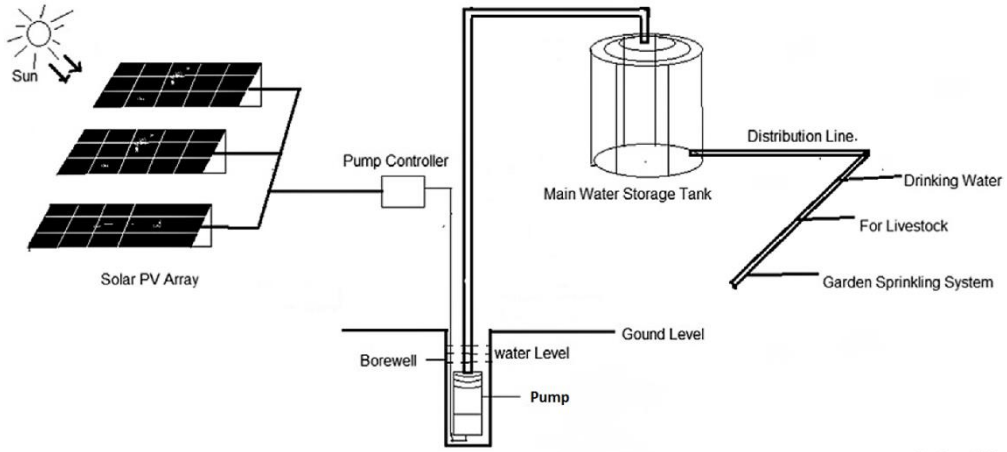

Figure 1.3: Schematic of direct-coupled solar PV water pumping system.

1.3.2.2 Based on the electric power input

The current generated by solar PV panel is DC. This can be converted into AC by an inverter. Accordingly, SWPS is classified as DC or AC driven.

- **DC SWPS**

In this type of SWPS, DC motor driven pump set is used as shown in Figure 1.4. The DC motor is of two types – conventional DC motor with brushes and brushless DC motor (BLDC). Conventional DC motor utilizes carbon brushes to transfer electric power from PV array to the motor shaft. These brushes wear out with the usage and need to be changed frequently. This increases operation and maintenance cost of the motor [10]. For Solar PV based application, BLDC motor can undoubtedly compete with any other motor for pumping application as it gives superior performance of motor along with soft starting. BLDC motor is the most advanced motor among the DC motors and they have almost same torque and speed usual curve uniqueness.

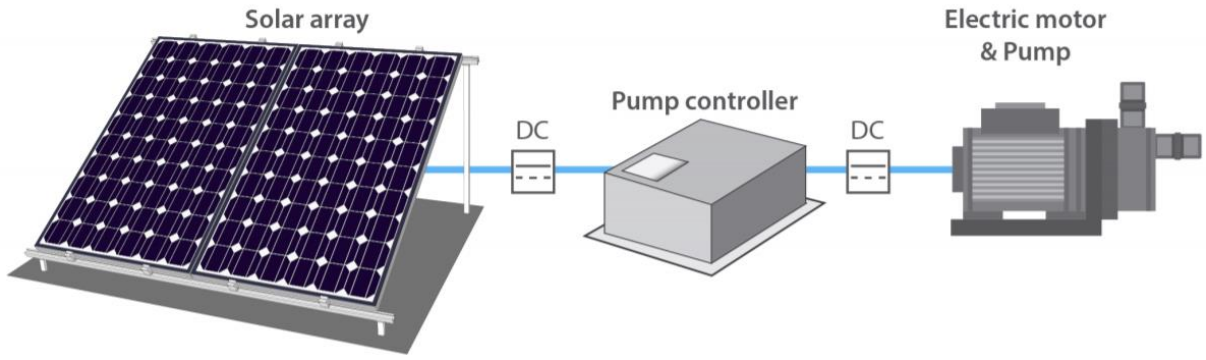

Figure 1.4: DC powered pump.

The ‘‘pump controller’’ in the DC powered pump system would typically include a maximum power point tracker (MPPT) to ensure that the solar array is delivering power at its peak power point.

- **AC SWPS**

Since the PV panel generates DC electricity, in AC SWPS, a suitable inverter is required to convert DC to AC electrical power. However, the use of inverter reduces the overall efficiency of SWPS. The advantage of the AC water pumping system is that it can run even on grid power in case of non-availability of PV power during night hours or during cloudy days. Induction and synchronous AC motors are used to run the pump [10].

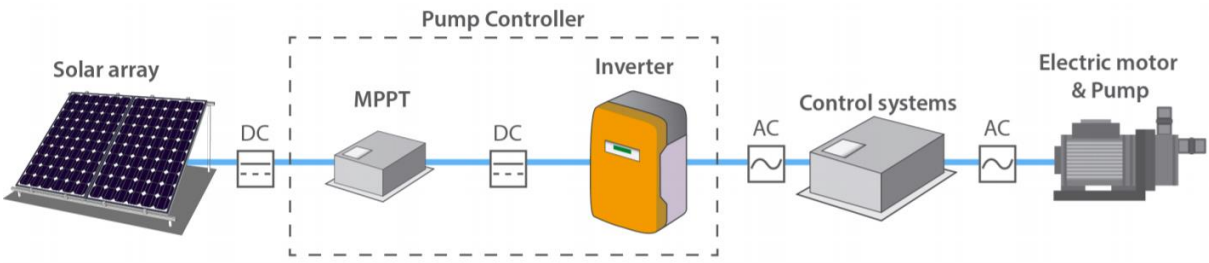

Figure 1.5: AC powered pump.

The "pump controller" in the AC powered pump system would include an MPPT as well as a DC to AC inverter in order to operate the AC electric motor which is part of the water pump as shown in Figure 1.5. In larger systems there should be three-phase inverters to operate three-phase motors.

1.3.2.3 Based on type of pump

The pumps are rated per voltage supplied and require sometimes accessories like filters, switches and float valves, to function optimally. Different configurations of SWPS are available according to the type of pump being used

- **Borehole/Well Pump (Submersible Pump)**

The most common water source in the Pacific is a borehole or well, fitted with a submersible pump. Figure 1.6 shows a typical borehole pump system. In these systems the solar water pump is located within the borehole or well. These pumps are generally available for 100 mm and 150 mm boreholes. The solar array is typically located near the top of the borehole/well and the water is generally pumped to a storage tank. The pump controller is typically located at the solar array. The pump and pump controller are interconnected using waterproof cables [15].

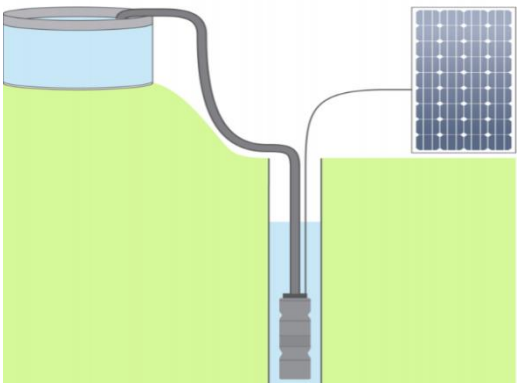

Figure 1.6: Borehole pump system

- **Surface Pump**

These systems are typically used in shallow wells or boreholes and also lakes, rivers and any open water source that is near or on the surface. The solar water pump is located above the water level and a suction pipe is used for drawing the water from the water source as is shown in Figure 1.7. In the Pacific they could be installed beside rivers and streams, though flooding may be a serious problem. It is not anticipated that there will be many sites associated with dams built specifically for the pumping system though that may be the case for some larger irrigation water supplies [15].

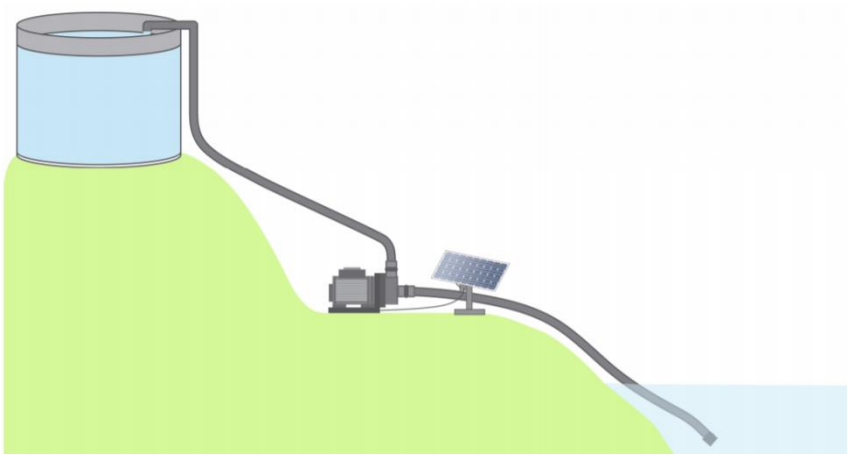

Figure 1.7: Surface pump system.

- **Floating Pump**

In these systems the water pump component is mounted within a floating device such that the pump inlet is located within the water source as shown in Figure 1.8. These systems remove any requirement for a suction pipe and the problems that can be associated with them, though a floating pump does usually require a flexible outlet pipe due to changes in the level of the water over time. The solar array is located on land near the pump and the water is typically pumped to a storage tank located well away from the actual water source. The pump controller is typically located near the solar array with the pump and pump controller interconnected using waterproof cables [15].

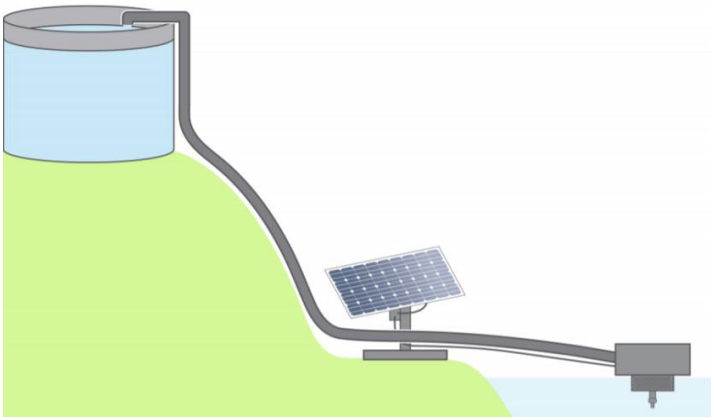

Figure 1.8: Floating pump system.

1. 4 Solar Pumping system description

Nowadays, the utilization of PV conversion of solar energy to power the water pumps is an emerging technology with great challenges. The PV technology can be applied on a larger scale and it also presents an environmentally favorable alternative to fossil fuel (diesel and electricity) powered conventional water pumps. Moreover, the importance of solar PV energy to power the water pumps increases due to the continuous depletion of oil reserves, uneven distribution and ever-increasing cost of electricity, which is a major area of concern for developing countries [12].

A PV pumping system is operated independently of the utility grid and it is composed of several components such as PV array, power converters, electrical motor, water pump and storage element which can be a battery bank or/and a water tank. PV pumping systems are generally installed with battery bank, and also can work without chemical storage elements. In battery-less PV pumping systems, the role of batteries is substituted by fluid storage, and steady-state operation depends on the amount of available power, in order to increase the reliability and decrease the cost of such systems (batteries are heavy and expensive and have short lifetime) [8].

The water pumps may be driven by many types of driving systems. The more popular are direct current (DC) motors, alternative current (AC) motors or Brushless DC motors. BLDC motor drives have received wide care as their performances superior to those of conventional brushed DC motors and AC motors. In small units up to 5.0 kW, BLDC motors are preferable and have increased the request in water pumping systems operated by a photovoltaic array because of their higher operating efficiency and good starting torque [13].

A typical configuration of solar-powered water pumping system is shown in Figure 1.9. The photovoltaic generator is a set of PV panels and their connection is chosen according to the power requirement of the association power electronic converters, motor and centrifugal pump. In PV systems, a DC/DC converter is installed between a PVG and pump which extracted the maximum energy during all the day. In order to extract the maximum power point tracking MPPT is used as online control strategy to track the maximum output power operating point of the PVG for different climatic conditions and it's important in SWPS because it reduces the solar array cost by decreasing the number of solar panels needed to obtain the desired output power [14].

In order to execute the control of the BLDC motor, an inverter must be included which provides three phase voltage and it can control the speed of the motor according the amplitude and frequency supplies depends of the water flow rate of the pump and variation of the climatic conditions.

The input variable of SWPS in this thesis is the solar irradiation and output variable is the water flow rate. The boost duty cycle by MPPT algorithm, which mainly depends on irradiance. Water flow rate depends on head and speed of the motor.

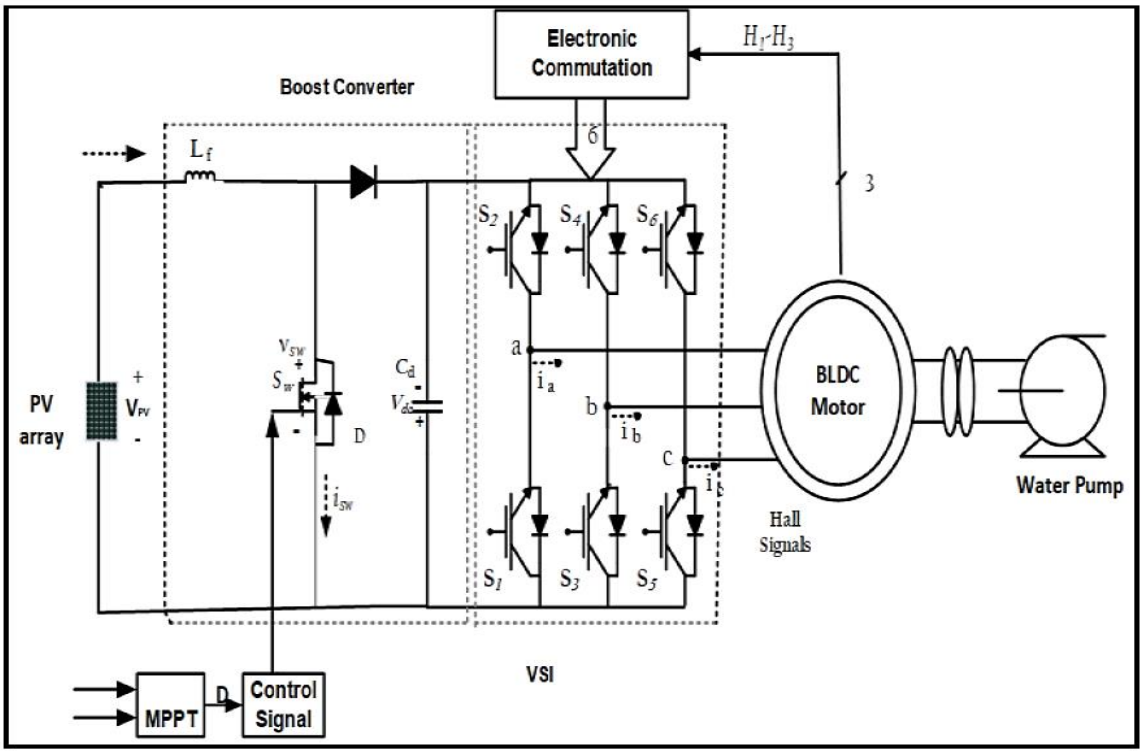

Figure 1.9: Configuration of the Solar PV array – boost converter fed BLDC motor driven water pump.

1.5 Conclusion

In this chapter, an introduction to Photovoltaic systems and Solar Water pumping systems have been presented including the different types of water pumping systems. Solar Water Pumping Systems (SWPS) were classified based on: the energy storage, the electric power input and the type of pump. Besides, the overall description of the system was presented.

Chapter 2

Modeling of the Photovoltaic Pumping System Components

2.1 Introduction

Following the discussion in the previous chapter, the battery-less photovoltaic (PV) water pumping system is a promising solution for an effective, economic and robust PV pumping system. The system includes a PV generation system, which is a group of series-parallel connected modules (PV array). A passive input filter, a capacitor, which is used to reduce the current and voltage ripple (and hence power) at the PV side, follows the PV array. The input filter is followed by a DC-DC boost converter, which is used to perform the maximum power point tracking (MPPT) of the PV array and elevate its voltage. The DC-DC converter is connected through a DC-link (capacitor) to the three-phase two-level inverter. The inverter is used to apply electronic commutation to the BLDC motor. The BLDC is directly coupled with a centrifugal pump in order to convert the mechanical energy to hydraulic energy. In order to control the PV pumping system, an essential step consists in modeling the installation components. Hence, this chapter presents the modeling of the proposed PV pumping system components. The mathematical models for PV array, both the boost and invert power converters, BLDC and centrifugal pump are explicitly developed.

2.2 Photovoltaic array modeling

The photovoltaic array consists of multiple photovoltaic modules connected in series and in series Parallel connection, where the basic components in the module are photovoltaic cells. The connection type depends on desired voltage and current levels dedicated to the power processing system running on the photovoltaic array. Figure 2.1 shows a photovoltaic array system.

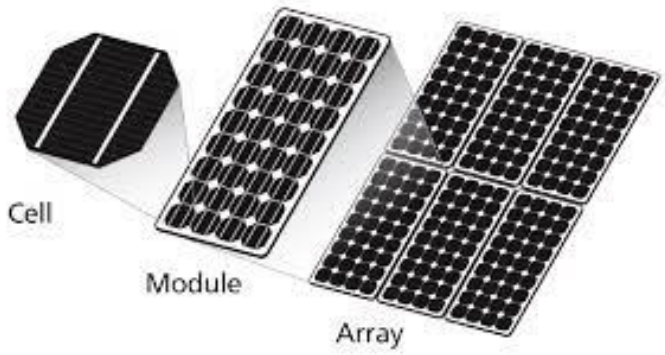

Figure 2.1: PV cell, module and array.

2.2.1 Photovoltaic Cell

In 1873, Willoughby Smith discovered that selenium had photo conductive potential, leading to William Grylls Adams' and Richard Evans Day's 1876 discovery, which states that selenium creates electricity when exposed to sunlight. A few years later in 1883, Charles Fritts produced the first solar cells made from selenium wafers – the reason some historians credit Fritts with the actual invention of solar cells. However, solar cells as we know them today are made with silicon, not selenium. Which is why some consider the true invention of solar panels to be tied to Daryl Chapin, Calvin Fuller, and Gerald Pearson's creation of the silicon photo-voltaic (PV) cell at Bell Labs in 1954 [16].

Photovoltaic (PV) cell, also known as a solar cell is basically a semiconductor diode whose p–n junction is exposed to light [17]. Photovoltaic cells are made of several types of semiconductors using different manufacturing processes. The monocrystalline and polycrystalline silicon cells are the only found at commercial scale at the present time. Silicon PV cells are composed of a thin layer of bulk Si or a thin Si film connected to electric terminals. One of the sides of the Si layer is doped to form the p–n junction. A thin metallic grid is placed on the Sun-facing surface of the semiconductor [18].

Si is not the only, and probably not the best, semiconductor material for PV cells, but it is the only one whose fabrication process is economically feasible in large scale. Other materials can achieve better conversion efficiency, but at higher and commercially unfeasible costs.

Today, the cost of PV cells is essential for the technology to further extend its use especially among utilities.

Solar cell uses semiconductor materials to convert sunlight into electricity. When these materials are exposed to light, they will absorb the photons that have a higher energy than the band gap energy of the semiconductor materials. This absorption of a photon knocks the electron free from their atom, allowing this electron to flow through the cell junction to produce electricity. This process of converting light energy (photons) to electricity (voltage) is called the photovoltaic effect as shown in Figure 2.2 [19].

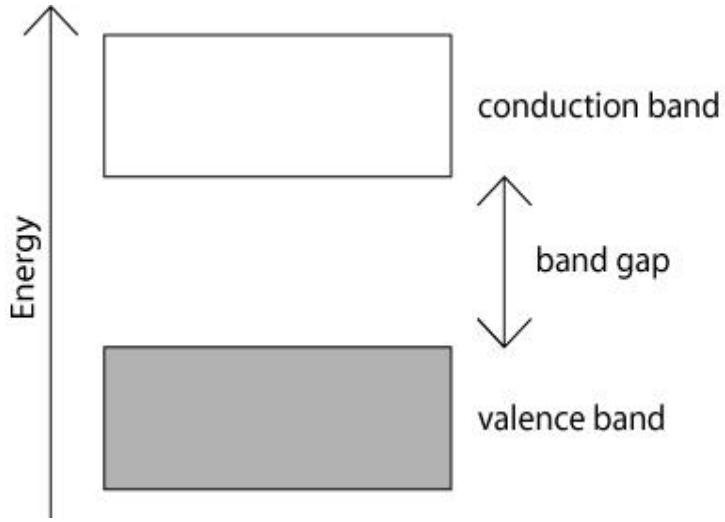

Figure 2.2: The semiconductor of converting light energy

Different equivalent circuit models of PV cell have been discussed in the literature [18. 20-23]. For simplicity and accuracy, the single diode model is the most studied and used in this work. The single-diode model includes four components: a photo current source, a diode parallel to the source, a series resistor R, and a shunt resistor R_{sh} [24].

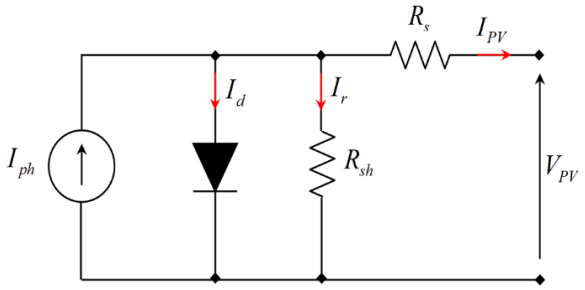

Figure 2.3: The equivalent circuit of a PV cell.

The model of Figure 2.3 can be mathematically described by the following equation [25]:

$$I_{PV} = I_{ph} - I_d - I_r = I_{ph} - I_o\left(e^{\frac{V_{PV}+R_sI_{PV}}{nV_t}} - 1\right) - \frac{V_{PV}+R_sI_{PV}}{R_{sh}} \quad (2.1)$$

Where: I_{PV}: is the cell output current (A).

I_{ph}: is the cell photocurrent (A).

I_d: is the diode current (Shockley equation) (A).

I_r: is the derived current by the shunt resistance (A).

I_o: is the reverse saturation current of the diode (A).

V_{PV}: is the cell output voltage (V).

R_s: is the cell series parasitic resistance (Ω).

R_{sh}: is the cell shunt parasitic resistance (Ω).

n: is the diode ideality factor

V_t: is the thermal voltage given by:

$$V_t = \frac{k\,T}{q} \tag{2.2}$$

where:

k: is the Boltzmann constant (1.38×10^{-23}J/K).

T: is the absolute temperature (k)

q: is the electronic charge (1.6×10^{-19} C)

2.2.2 Photovoltaic module

Due to low power ratings of each individual PV cell, the cells are connected in series-parallel configuration form a PV module in order to produce the required power. Usually, the PV module is rated by its DC output power under standard test conditions (STC) and commercially STC is specified at an irradiance of 1000 W/m2 and a 25°C PV cell temperature [25]. Figure 2.4 shows the equivalent circuit of a PV module. The nonlinear current-voltage characteristic of the PV module is modeled by the following equation where all cells are identical [25]:

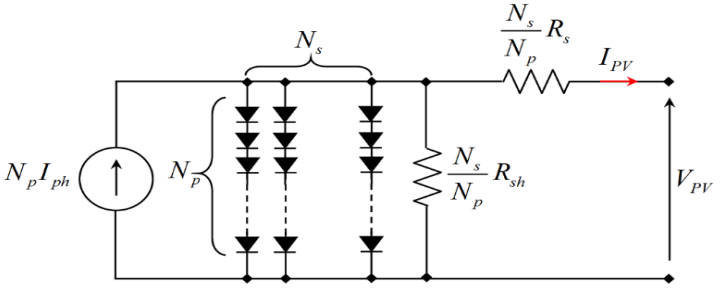

Figure 2.4: The equivalent circuit of a PV module.

Where:

I_{PV}: is the module output current (A).

V_{PV}: is the module output voltage (V).

N_s: is the number of cells connected in series

N_p: is the number of cells connected in parallel

The PV module considered for this thesis is Trina Solar TSM-250PA05.08 PV model. The power versus voltage (P-V) and the current versus voltage (I-V) characteristics of Trina Solar TSM-250PA05.08 PV model under STC are shown in Figure 2.5. A PV module can produce the power at a point, called an operating point, anywhere on the I-V curve. Three operating points on the I-V curve are important in defining the performance of a PV module, i.e., the maximum power point, short-circuit current and the open-circuit voltage.

- The maximum power point (MPP) is the point on the I-V curve at which the PV module works with maximum power output.
- The short-circuit current point characterized by a zero voltage at the PV module terminals and by a short-circuit current (I_{sc}).
- The open-circuit voltage point characterized by a zero current in the PV panel terminals and by an open-circuit voltage (V_{OC}).

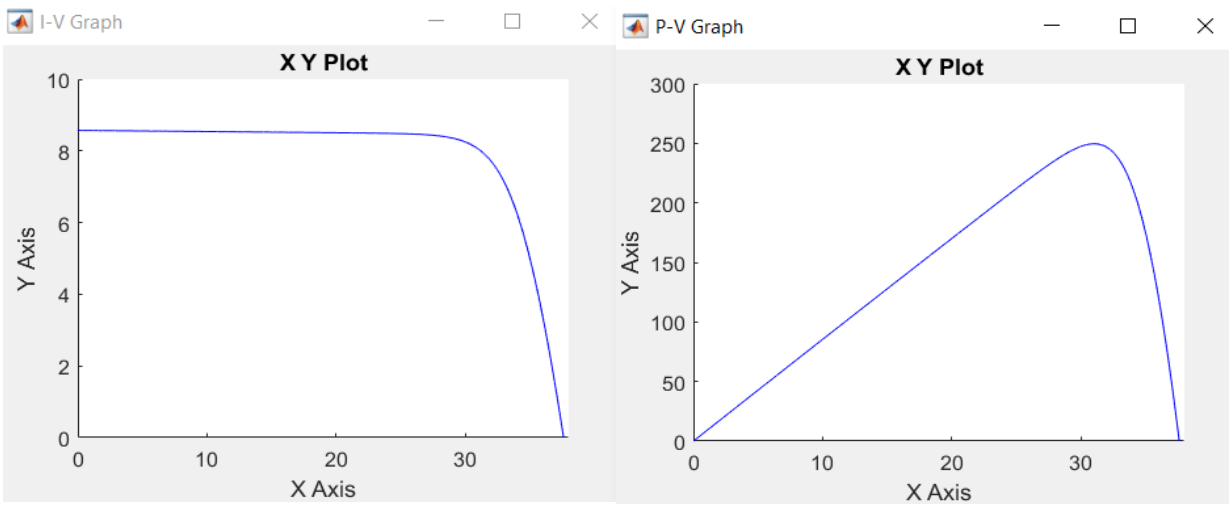

(a) (b)

Figure 2.5: (a) I-V and (b) P-V characteristics of the solar Trina Solar TSM-250PA05.08 PV model under STC.

2.2.3 Photovoltaic array

A PV array is made of a number of PV modules connected in series-parallel arrangement to obtain the desired voltage, current and power. The size of the PV array varies from a single PV module to any number of modules. The PV array output current and voltage can be computed from equations (2.3) and (2.4) respectively [26]:

$$I_{PVt} = N_{pp}\, I_{PV} \tag{2.3}$$

$$V_{PVt} = N_{ss}\, V_{PV} \tag{2.4}$$

where:

I_{PVt} : is the array output current (A).

V_{PVt} : is the array output voltage (V).

I_{PV}: is the module output current (A).

V_{PV}: is the module output voltage (V).

N_{ss}: is the number of modules connected in series.

N_{pp}: is the number of modules connected in parallel.

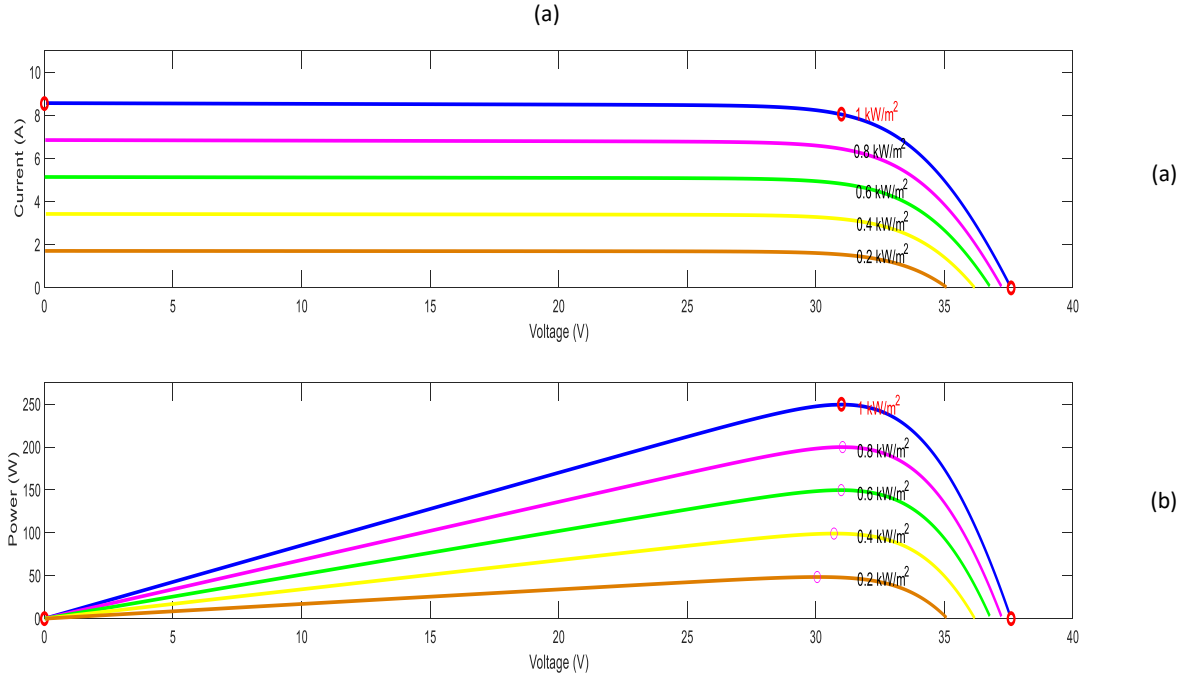

Figure 2.6: (a) I-V and (b) P-V characteristics of PV array under different levels of solar irradiation at 25°C.

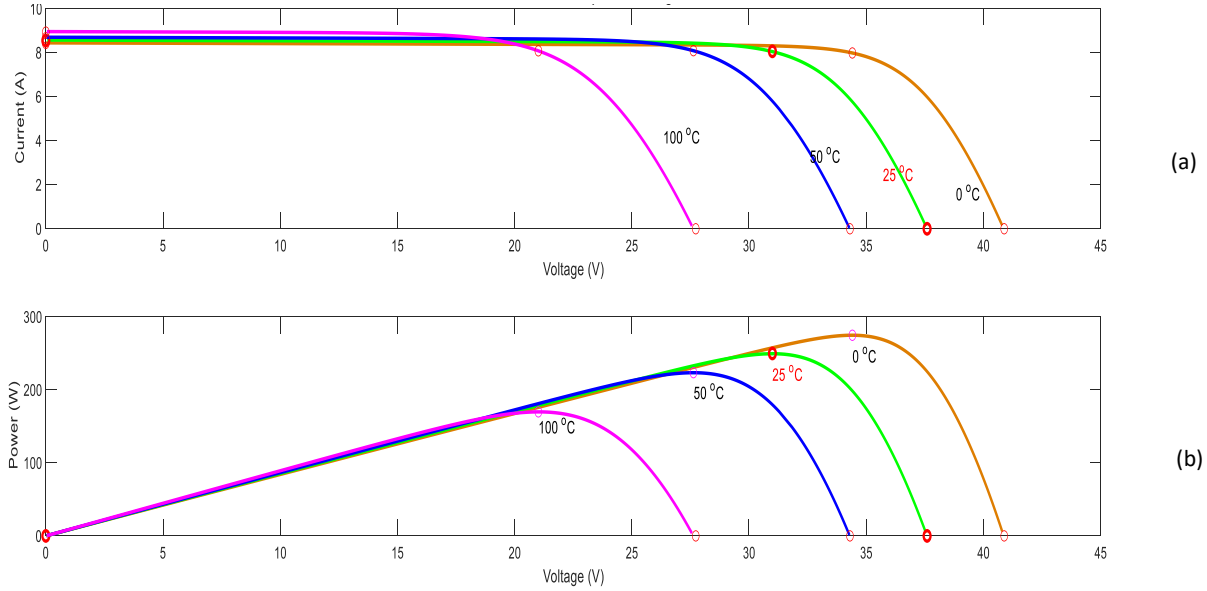

Figure 2.7: (a) I-V and (b) P-V characteristics of PV array under different temperatures at 1000 W/m2.

The electrical behavior of the PV array is generally represented by the power versus voltage (P-V) and the current versus voltage (I-V) characteristics. A TSM-250PA05.08 PV model is considered. Figures 2.6 and 2.7 highlighted the strong dependence of the considered PV model performances on the temperature and irradiance levels. The irradiance has a significant effect on the short-circuit current value, as shown in Figure 2.6.

On the contrary, the irradiance level has a slight effect on the open-circuit current value. On the other hand, the temperature has a negligible effect on the short-circuit value but it has an important effect on the open circuit voltage value, as shown in Figure 2.7. It is worth nothing that the temperature usually changes quite slowly, so that the temperature value is often considered a constant with respect to the variation in the irradiation level that can be subjected to during the day. This simplifying assumption will be also adopted in this thesis.

2.3 Power Converters modeling

The power electronic converters used in the PV system are receiving more attention due to their flexible controllability and maturing technology. They are used as an interface between the PVG and the load in photovoltaic systems. For a PV array, the output power is a DC power and variable as the climatic conditions change. A DC-DC boost converter is deployed to optimize the operating power of the PV array, speed control of the BLDC motor-pumping and soft starting. A voltage source inverter (VSI) is needed to control the operation of the BLDC motor.

2.3.1 DC-DC Boost Converter

A DC/DC converter acts as an interface between the load and the PV module. It is widely used in DC power supplies and DC motor drives for the purpose of converting unregulated DC input into a controlled DC output at a desired voltage level [27]. Usually the MPPT controls a DC/DC converter that is generally placed between the PV array and the inverter, to maintain a constant DC voltage at the output of the generator. [28]

The boost topology is used for stepping up the voltage when they are connected to utility mains through an inverter stage. In this type of converter, the output voltage is always greater than the input voltage [29]. Therefore, the step-up chopper can be applied to MPPT systems where the output voltage needs to be greater than the input voltage [30]. The circuit topology is shown in Figure 2.8.

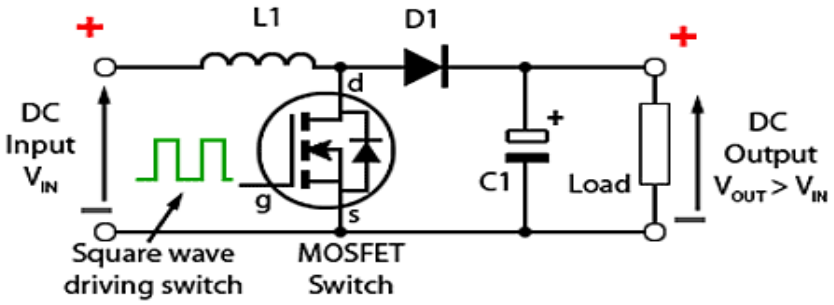

Figure 2.8: Boost converter

The waveform of the current and voltage of the Boost converter during continuous conduction mode is shown below in Figure 2.9 [31].

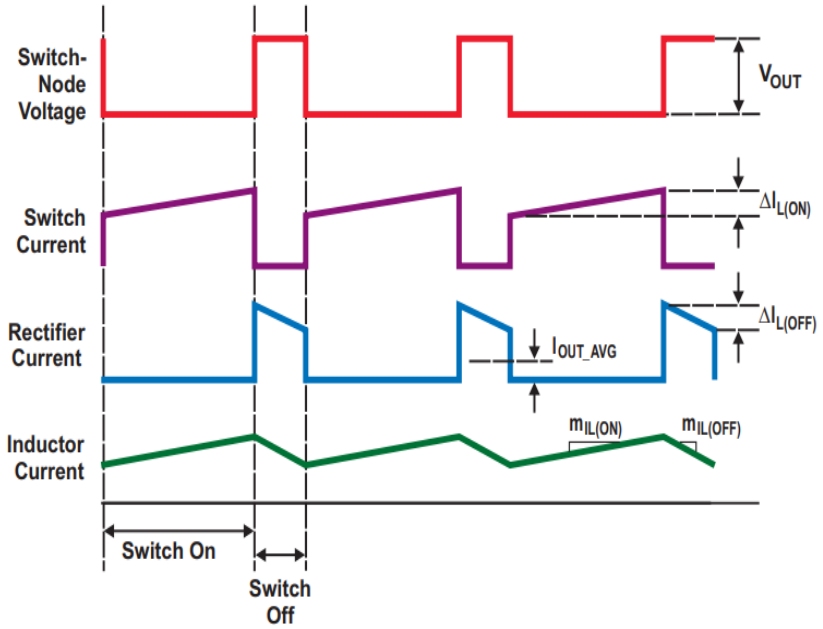

Figure 2.9: Circuit schematic of Boost converter [32]

The equivalent boost circuits during switch-on and switch-off intervals for ideal switch are shown in Figure 2.10.

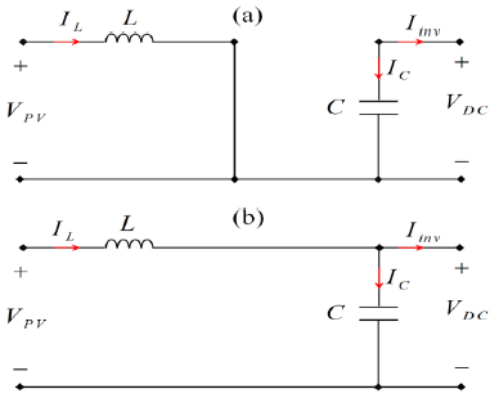

Figure 2.10: Equivalent boost circuits: (a) switching on and (b) switching off.

When the switch is considered as closed as shown in Figure 2.10(a), the boost converter operation can be described by the well-known system of equations as follows:

$$\frac{d}{dt}I_L = \frac{1}{L}V_{PV} \tag{2.5}$$

$$\frac{d}{dt}V_{DC} = -\frac{1}{C}I_{inv} \tag{2.6}$$

In case of the open switch (Figure 2.10(b)), the previous equation system can be expressed as:

$$\frac{d}{dt}I_L = \frac{1}{L}(V_{PV} - V_{DC}) \tag{2.7}$$

$$\frac{d}{dt}V_{DC} = \frac{1}{C}(I_L - I_{inv}) \tag{2.8}$$

The aforementioned equations (Eq. 2.5 to 2.8) can be expressed as follows:

$$\frac{d}{dt}I_L = -(1 - \mathrm{S})\frac{1}{L}V_{DC} + V_{PV} \tag{2.9}$$

$$\frac{d}{dt}V_{DC} = (1 - \mathrm{S})\frac{1}{C}I_L - \frac{1}{C}I_{inv} \tag{2.10}$$

Where:

L_I: is the boost input current (A).

V_{PV}: is the boost input voltage (V).

V_{DC}: is the boost output voltage (V).

inv I: is the boost output current (A).

L: is the boost input inductor (mH).

C: is the boost output capacitor (μF).

S: is the switching signal taking value from the discrete set

S = [1,0].

2.3.2 VSI inverter

Inverter in Power-Electronics pertains to a class of power transition circuits that run from a DC voltage source or a DC current source and convert it into an AC voltage or current. It is the opposite of ac-to-dc converter. The input to the inverter is DC source or DC source deduced from an AC voltage source [33]. Figure 2.11 represents the power circuit of a three-phase VSI.

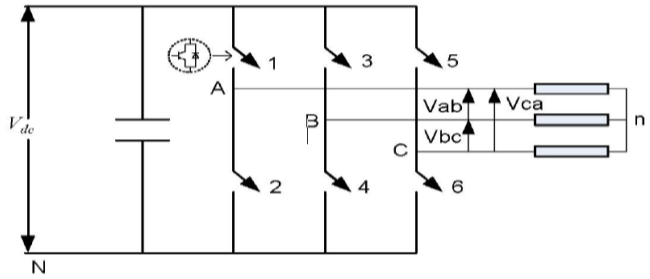

Figure 2.11: Power circuit of a three-phase VSI.

- **Three-phase VSI modelling review**

Mathematical model of a three-phase VSI is presented here based on space vector representation. The power circuit Space vector representation of the three-phase VSI was shown in Figure 2.11. Each switch in the inverter leg is composed of two back-to-back connected semiconductor devices. One of these two is a controllable device and the other one is a diode for protection. Leg voltage waveforms are shown in Figure 2.12 for 180° conduction mode [34].

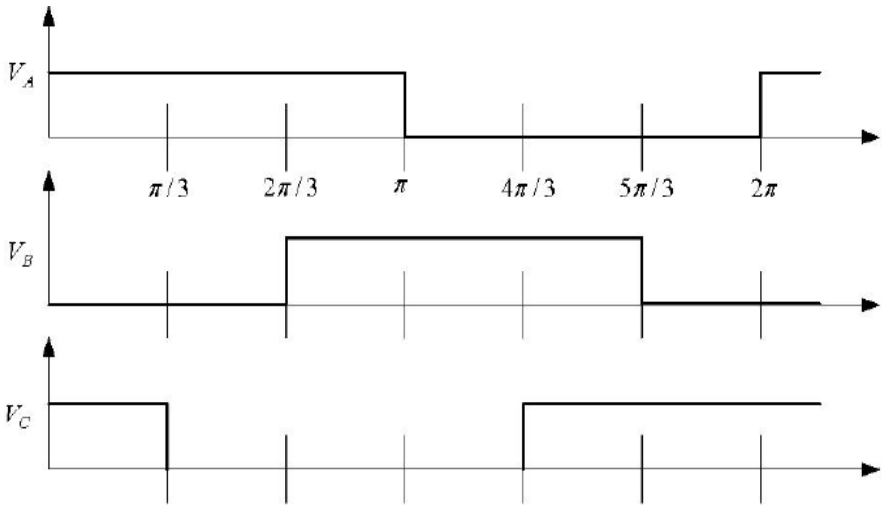

Figure 2.12: Leg voltage waveform of a three-phase VSI.

It is observed from Figure 2.12 that one inverter leg's state changes after an interval of 60° and their state remains constant for 60° interval. Thus, it follows that the leg voltages will have six distinct and discrete values in one cycle (360°). Space vector representation of the three-phase inverter output voltages is introduced next. Space vector is defined as:

$$\overrightarrow{Vs} = \frac{2}{3}(Va + \bar{a}\,Vb + \bar{a}^2\,Vc) \tag{2.11}$$

where $\bar{a}$ =exp (j2 π /3). The space vector is a simultaneous representation of all the three-phase quantities. It is a complex variable and is a function of time in contrast to the phasors. Phase-to-neutral voltages of a star-connected load are most easily found by defining a voltage difference between the star point n of the load and the negative rail of the dc bus N. The following correlation then holds true:

$$V_A = V_a + V_{nN};$$
$$V_B = V_b + V_{nN};$$
$$V_C = V_c + V_{nN} \tag{2.12}$$

Since the phase voltages in a start connected load sum to zero, summation of equation (2.12) yields:

$$V_{nN} = (1/3)\,(V_A + V_B + V_C) \tag{2.13}$$

Substitution of (2.13) into (2.12) yields phase-to-neutral voltages of the load in the following form:

$$V_a = (2/3)\,V_A - (1/3)\,(V_B + V_C);$$
$$V_b = (2/3)\,V_B - (1/3)\,(V_A + V_C);$$
$$V_c = (2/3)\,V_C - (1/3)\,(V_B + V_A) \tag{2.14}$$

Phase voltages are summarized in Table 1 and their corresponding space vectors are listed in Table 2.2.

Table 2.1: Phase voltage values for different switching states

State	Switch On	V_A	V_B	V_C
1	1,4,6	(2/3) V_{dc}	-(1/3) V_{dc}	-(1/3) V_{dc}
2	1,3,6	(1/3) V_{dc}	(1/3) V_{dc}	-(2/3) V_{dc}
3	2,3,6	-(1/3) V_{dc}	(2/3) V_{dc}	-(1/3) V_{dc}
4	2,3,5	-(2/3) V_{dc}	(1/3) V_{dc}	(1/3) V_{dc}
5	2,4,5	-(1/3) V_{dc}	-(1/3) V_{dc}	(2/3) V_{dc}
6	1,4,5	(1/3) V_{dc}	-(2/3) V_{dc}	(1/3) V_{dc}
7 & 8	1,3,5 2,4,6	0	0	0

Table 2.2: Phase voltage space vectors

State	Phase voltage space vectors
1	(2/3) V_{dc}
2	(2/3) V_{dc} exp (jπ/3)
3	(2/3) V_{dc} exp (j2π/3)
4	(2/3) V_{dc} exp (jπ)
5	(2/3) V_{dc} exp (j4π/3)
6	(2/3) V_{dc} exp (j5π/3)
7&8	0

The discrete phase voltage space vector positions are shown in Figure 2.13.

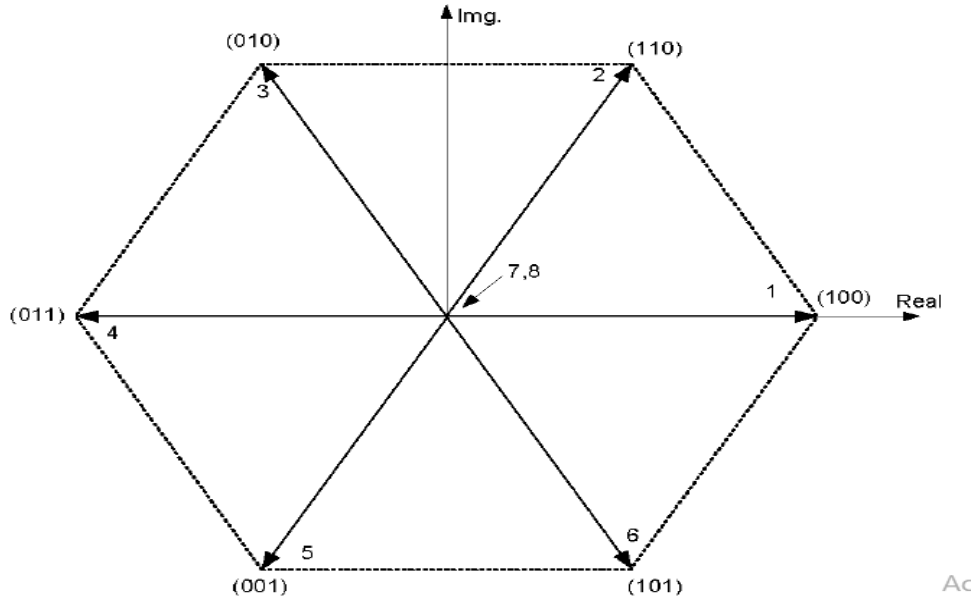

Figure 2.13: Phase voltage space vectors.

The binary numbers on the figure indicate the switch state of inverter legs. Here 1 implies upper switch being on and 0 refers to the lower switch of the leg being on. The most significant bit is for leg A, the least significant bit is related to leg C and the middle is for leg B [35].

2.4 Brushless DC motor

The Brushless DC motors (BLDC motors or BL motors), also known as electronic commutation motors (ECM or EC motors) or synchronous DC motors, are synchronous motors that use direct current (DC) power. The BLDC motor has no brushes on the rotor and the commutation is performed electronically at certain rotor positions. The stator phase windings are inserted in the slots (a distributed winding), or can be wound as one coil on the

magnetic pole. The magnetization of the permanent magnets and their displacement on the rotor are chosen in such a way that the back-EMF shape is trapezoidal. This allows the three-phase voltage system, with a rectangular shape, to be used to create a rotational field with low torque ripples. In this respect, the BLDC motor is equivalent to an inverted DC commutator motor in that the magnets rotates while the conductors remain stationary [36].

The torque of the BLDC motor is mainly influenced by the waveform of back-EMF (the voltage induced into the stator winding due to rotor movement). The ratio of the torque delivered to the size of the motor is higher, making it useful in applications where space and weight are critical factors [37].

Ideally, the BLDC motors have trapezoidal back-EMF waveforms and are fed with rectangular stator currents, which give a theoretically constant torque. However, in practice, torque ripple exists, mainly due to emf waveform imperfections, current ripple and phase current commutation. The current ripple result is from PWM or hysteresis control.

2.4.1 Why using BLDC motor to drive the solar pump

A motor plays prominent role to realize a solar PV based energy efficient and cost-effective water pumping. An efficient motor drastically minimizes the number of solar modules for a given power demand and hence its capital cost. The DC motors are mostly used in a low power solar PV water pumping. The DC motor with brushes possesses a low efficiency, and it requires regular maintenance due to the sliding brush contacts and the commutator. An induction motor-based PV pumping system is reliable, rugged and maintenance-free with better efficiency and offers more flexibilities for control in comparison to DC motors. The brushless DC (BLDC) motor is identified as a better substitute of the DC motor and an induction motor for PV fed water pumping. This motor is compact, rugged and efficient in comparison to an AC motor. Moreover, a BLDC motor possesses several merits such as reliability, least maintenance requirement, a wide range of speed, easy-to-drive and simple control. Therefore, this motor has received increased attention for water pumping in the last decade owing to its various merits which constitute the attractive features particularly for this application [38].

Table 2.3: Advantages and disadvantages of the different types of motors used for PV water pumping system [39].

Motor	Advantages	Disadvantages
AC motor	Simple design Low cost Reliable	Expensive speed control Bad at low speeds Poor positioning control
DC motor	Easy and simple design Easy speed control Torque control	Hard control and low speed High maintenance Dusty (brushes)
BLDC	High efficiency Low maintenance Long life Low noise Low weight	Need sensor for position High cost

2.4.2 Mathematical model of the BLDC motor

Modeling of a BLDC motor can be developed in the similar manner as a three-phase synchronous machine. Since there is a permanent magnet mounted on the rotor, some dynamic characteristics are different. Flux linkage from the rotor depends upon the magnet material. Therefore, saturation of magnetic flux linkage is typical for this kind of motors. As any typical three-phase motors, one structure of the BLDC motor is fed by a three-phase voltage source. The source is not necessarily to be sinusoidal. Square wave or other wave-shape can be applied as long as the peak voltage does not exceed the maximum voltage limit of the motor. Similarly, the model of the armature winding for the BLDC motor [36] is expressed as follows:

$$V_a = Ri_a + L\frac{di_a}{dt} + e_a \quad (2.15)$$

$$V_b = Ri_b + L\frac{di_b}{dt} + e_b \quad (2.16)$$

$$V_c = Ri_c + L\frac{di_c}{dt} + e_c \quad (2.17)$$

Where:

L is armature self-inductance [H],

R - armature resistance [Ω],

V_a, V_b, V_c - terminal phase voltage [V],

i_a, i_b, i_c - motor input current [A], and e_a, e_b, e_c - motor back-EMF [V].

In the 3-phase BLDC motor, the back-EMF is related to a function of rotor position and the back-EMF of each phase has 120º phase angle difference so equation of each phase should be as follows[36]:

$$e_a = K_W f(\theta_e)\,\omega \quad (2.18)$$

$$e_b = K_W f(\theta_e - 2\pi/3)\,\omega \quad (2.19)$$

$$e_c = K_W f(\theta_e + 2\pi/3)\,\omega \quad (2.20)$$

Where:

K_w is back EMF constant of one phase [V/rad.s^{-1}],

θ_e - electrical rotor angle [° el.],

ω - rotor speed [rad.s^{-1}].

The electrical rotor angle is equal to the mechanical rotor angle multiplied by the number of pole pairs *p*

$$\Theta_e = \frac{P}{2}\Theta_m \quad (2.21)$$

Where:

θ_m is mechanical rotor angle [rad].

Total torque output can be represented as summation of that of each phase. Next equation represents the total torque output:

$$T_e = \frac{e_a\, i_a + e_b\, i_b + e_c\, i_c}{\omega} \quad (2.22)$$

Where:

*T*e is total torque output [Nm].

The equation of mechanical part is represented as follows:

$$T_e - T_l = J\frac{d\omega}{dt} + B\omega \quad (2.23)$$

Where:

T_l is load torque [Nm],

J - inertia of rotor and coupled shaft [kgm^2],

B - friction constant [Nms.rad^{-1}].

2.4.3 Hall effect sensor

The Hall effect was discovered by Dr. Edwin Hall in 1879 while he was a doctoral candidate at Johns Hopkins University in Baltimore. Hall was attempting to verify the theory of electron flow proposed by Kelvin some 30 years earlier. Dr. Hall found when a magnet was placed so that its field was perpendicular to one face of a thin rectangle of gold through which current was flowing, a difference in potential appeared at the opposite edges. He found that this voltage was proportional to the current flowing through the conductor, and the flux density or magnetic induction perpendicular to the conductor. Although Hall's experiments were

successful and well received at the time, no applications outside of theoretical physics were found for over 70 years until the 1950s.

When a current-carrying conductor is placed into a magnetic field, a voltage will be generated perpendicular to both the current and the field. This principle is known as the Hall effect. Hall effect sensors can be applied in many types of sensing devices. If the quantity (parameter) to be sensed incorporates or can incorporate a magnetic field, a Hall sensor will perform the task [40].

The Hall effect is an ideal sensing technology. The Hall element is constructed from a thin sheet of conductive material with output connections perpendicular to the direction of current flow. When subjected to a magnetic field, it responds with an output voltage proportional to the magnetic field strength. The voltage output is very small (μV) and requires additional electronics to achieve useful voltage levels. When the Hall element is combined with the associated electronics, it forms a Hall effect sensor. The heart of every MICRO SWITCH Hall effect device is the integrated circuit chip that contains the Hall element and the signal conditioning electronics. Although the Hall effect sensor is a magnetic field sensor, it can be used as the principal component in many other types of sensing devices (current, temperature, pressure, position, etc.). Figure 2.14 shows a block diagram of a sensing device that uses the Hall effect. In this generalized sensing device, the Hall sensor senses the field produced by the magnetic system. The magnetic system responds to the physical quantity to be sensed (temperature, pressure, position, etc.) through the input interface. The output interface converts the electrical signal from the Hall sensor to a signal that meets the requirements of the application. [41]

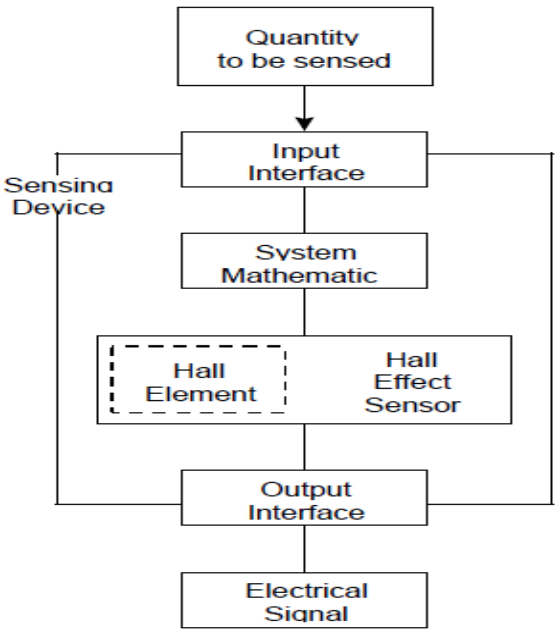

Figure 2.14: General sensor based on the Hall effect [41]

When a current-carrying conductor is placed into a magnetic field, a voltage will be generated perpendicular to both the current and the field. This principle is known as the Hall effect. Hall effect sensors can be applied in many types of sensing devices. If the quantity (parameter) to be sensed incorporates or can incorporate a magnetic field, a Hall sensor will perform the task. Figure 2.15 presents the classical Greek-cross shape of a Hall Effect sensor. We can observe the symmetrical and orthogonal character of the shape. The figure also depicts the biasing and sensing contacts. If a current is applied between two contacts (let us say b and d) and the probe is placed under a magnetic field, the carriers will be deviated by the Lorentz force and a voltage drop which is called the Hall voltage will appear between the other two opposite contacts (a and c) [42].

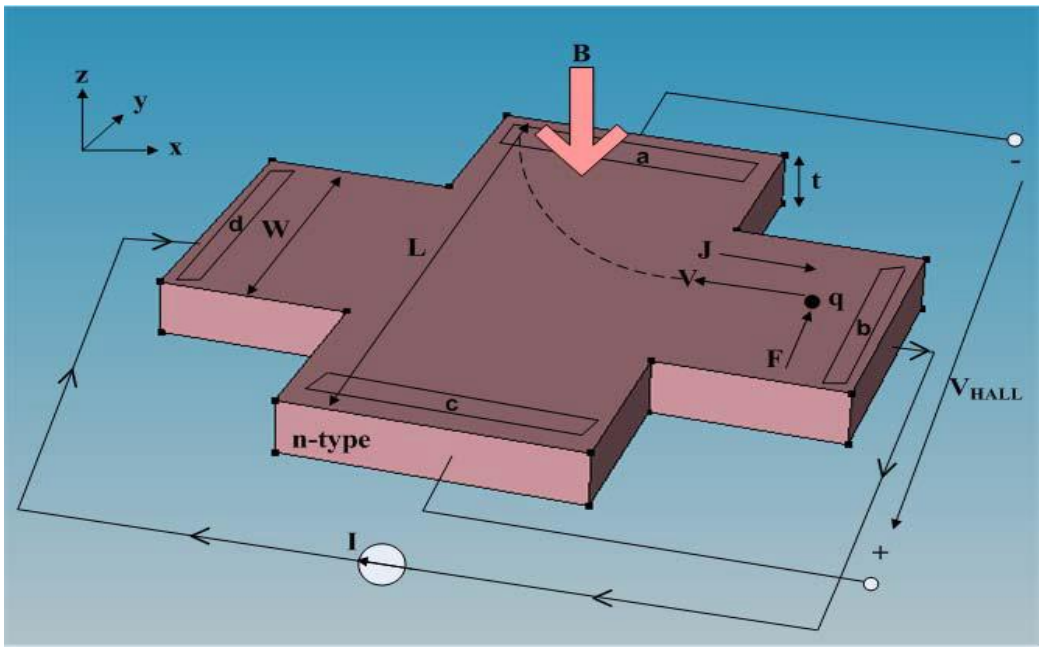

Figure 2.15: Classical Greek-cross Hall Effect sensor representation.

In Hall Effect sensors performance assessment, the Hall voltage and sensitivity are important parameters. By consequence, the Hall voltage is defined by the relation:

$$V_{hall} = G\,\frac{r_H}{nqt} I_{Bias}\, B \tag{2.24}$$

where G is the geometrical correction factor, r_H is the scattering factor of Silicon, (usually 1.15), n is the carrier density, t is the thickness of the active region, I_{bias} is the biasing current, and B is the magnetic field induction [43].

2.5 Centrifugal Pump

Pumps are essential equipment in many industries including power and chemical, mineral and mining, manufacturing, heating, air conditioning and cooling. Centrifugal pump is a mechanical device that converts mechanical energy into pressure energy by means of centrifugal force acting on the fluid. It has relatively high efficiency and are capable of pumping a high volume of water [44].

In our SWPS, a dynamic pump (centrifugal) has been selected as it requires less maintenance and offers better ability to match with output of PV generators.

The torque of the pump is proportional to the square of the rotor speed:

$$T_L = K_P \Omega_r^2 \tag{2.25}$$

where K_P is the proportionality constant and it is given by:

$$K_p = P_{np} / \Omega_{rn}^3 \tag{2.26}$$

The water rate and pressure of the pump depend on the available mechanical power at the rotating impeller and the total head. The determination of the pump's output parameters can be simplified using affinity laws which require only pump ratings and actual input parameters; rotor speed and torque [44].

The Affinity Laws

Processes require the satisfaction of the hydraulic parameters of head and flow rate. The Affinity Laws are mathematical relationships that allow for the estimation of the changes in the pump performance curves as a result of a change in the shaft speed (N) or in the impeller diameter.

Fixing the impeller diameter, the Affinity Laws state that for a given pump, the flow rate (Q) will be directly proportional to the speed, the head (H) will be directly proportional to the square of the speed, and the required power (P) will be directly proportional to the cube of the speed [45] :

$$\frac{Q_1}{Q_2} = \frac{N_1}{N_2};$$
$$\frac{H_1}{H_2} = \left(\frac{N_1}{N_2}\right)^2;$$
$$\frac{P_1}{P_2} = \left(\frac{N_1}{N_2}\right)^3 \tag{2.27}$$

2.6 Conclusion

The aim of this chapter is to describe the components models of the proposed battery-less photovoltaic pumping system, which will be used in the following chapters for the system control and simulation work. First, the photovoltaic cell, module and array, and their characteristic curves have been described. Additionally, the power converters used in the proposed pumping system were presented to illustrate their power circuit and to model mathematically. Moreover, the BLDC motor is modeled to facilitate and understand the operation of motor control. Finally, the centrifugal pump model and the affinity laws were presented.

Chapter 3

BLDC-based Solar water Pumping system control

3.1 Introduction

Maximum power point tracking (MPPT) techniques play an essential role in efficiency improvement of photovoltaic (PV) systems. The perturb and observe (P&O) technique is the most popular MPPT algorithm for industry applications due to the good balance between complexity, accuracy and reliability. However, the P&O usually presents some drawbacks such as slow response speed, steady-state power oscillation around the MPP and the poor tracking under sudden irradiance changes.

In this context, Particle Swarm Optimization (PSO) and Cuckoo Search (CS) algorithms are presented in order to minimize the problems mentioned above. Besides, the control techniques of the BLDC motor are presented focusing on the hall effect sensor and VSI drive along with the speed control.

3.2 Maximum Power Point Tracking Algorithms

3.2.1 Under normal conditions

MPPT algorithms are necessary in PV applications because the MPP of a solar panel varies with the weather conditions, such as solar irradiation, shadow, and temperature. To extract the maximum power, it is necessary to implement an MPPT algorithm that dynamically adjusts the extraction of the power. Convergence speed is one of the most important features among all different MPPT algorithms. Such that, any improvement in the rise time of MPPT improves the reliability of the system and increases the power extraction and efficiency of the whole system [46].

- **Perturb and Observe (P&O)**

This algorithm is a simple iterative technique. It does not require previous knowledge of the PV generator characteristics or the measurement of solar intensity and cell temperature and it is easy to implement with analogue and digital circuits. It perturbs the operating point of the system causing the PV array terminal voltage to fluctuate around the MPP voltage even if the solar irradiance and the cell temperature are constants [46].

It measures the panel operating voltage and current periodically and calculates the instantaneous power P(k). This instantaneous power compares with the previous output power P(k)-P(k-1), then the operating voltage V(k+1) is determined and changed by changing the duty ratio of the converter V(k+inc) or V(k-inc). The sign of change of output power is also observed to track the MPP. If the output power increases by increasing the operating voltage, then the operating voltage is further perturbed in the same direction until it reaches the point of MPP or dp/dv=0. If the output power decreases by increasing the operating voltage, i.e the operating point is in the negative slope region of the PV curve. Then the operating voltage is perturbed in the reverse direction to track the MPP [47] . Figure 3.1 shows the P&O algorithm flowchart.

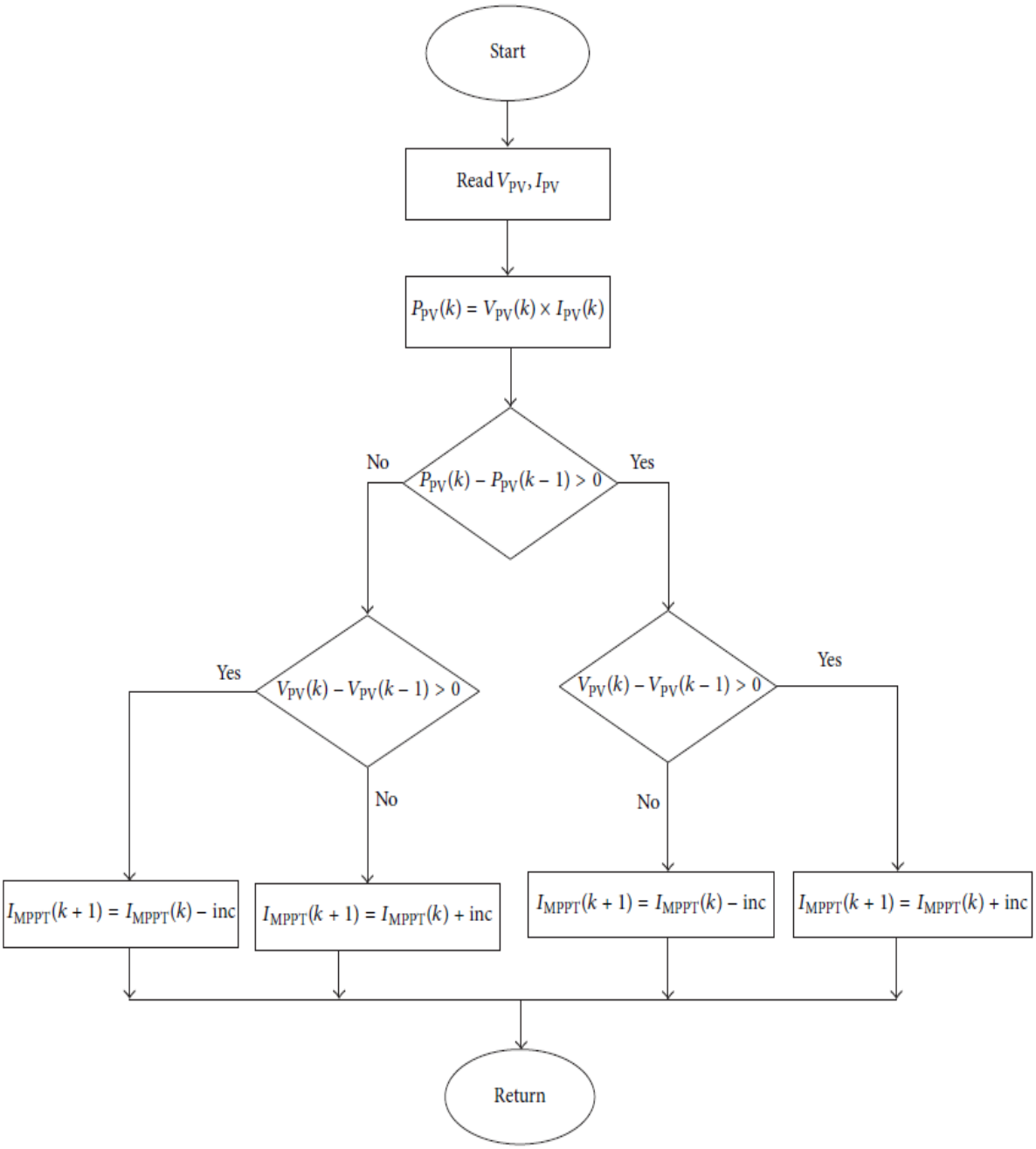

Figure 3.1: Flowchart of P&O Algorithm [46].

Moreover, P&O algorithm is the most widely used MPPT algorithm due to its balance between performance and simplicity. However, it suffers from the lack of speed and adaptability which is necessary for tracking the fast transients under varying environmental conditions. It is simple and straightforward technique but degraded performance is achieved due to the trade-off between accuracy and speed upon selecting the step size [46].

3.2.2 Under partial shading effect

Depending on the power demand, solar panels are connected to each other in series or parallel. Thus, electrical energy from the solar array systems is created to meet the needs. Solar

panels are used on roof and wall systems in buildings and power plants. In solar array design, radiance, temperature, shading, surface angle and effect of series-parallel connection, which are factors affecting the operation of solar panels, should be considered. Shading significantly reduces the efficiency of a solar array system. Shading can occur entirely or partially due to dynamic or static obstacles. The effect of shading varies by location at which the solar panel is formed [48] as shown in Figure 3.2.

Figure 3.2: PV system under partial shading.

In a PV module the shading does not decrease the power only however it leads into current mismatch within a PV series string and voltage mismatch among parallel strings. A cell can be treated as a combination of a current generator connected with a diode. The photo-current flows in the invert leading of the diode, which means that if one cell s partially shaded, it will product minimal current than the other cells in the string, and the else cells will seek to supply extra current during the bad cell than the poor cell deliver. However, this is not possible ago

then the cell works as a diode in the invert trend. Then the current produced in the poor cell will border the current in the string [49]. Then the shaded cells then operate with a reverse bias voltage to provide the same current as the remaining cells. However, the resulting reverse power polarity leads to power consumption and a reduction in the maximum output power of the partially shaded PV module which causes a hot spot to appear on them and creating an open circuit in the entire PV module. In order to avoid power damage and hot spot trouble in the panel during the partial shading a bypass diode is connected in parallel with the PV module [50].

- **Bypass diodes**

The use of bypass diodes allows a series (called a string) of connected cells or panels to continue supplying power at a reduced voltage rather than no power at all. In general, as shown in Figure 3.3 Bypass diodes are connected in reverse bias between a solar cells (or panel) positive and negative output terminals and has no effect on its output. Bypass diodes are used in parallel with either a single or a number of photovoltaic solar cells to prevent the current flowing from well-exposed to sunlight solar cells overheating weaker or partially shaded solar cells by providing a current path around the bad cell [51].

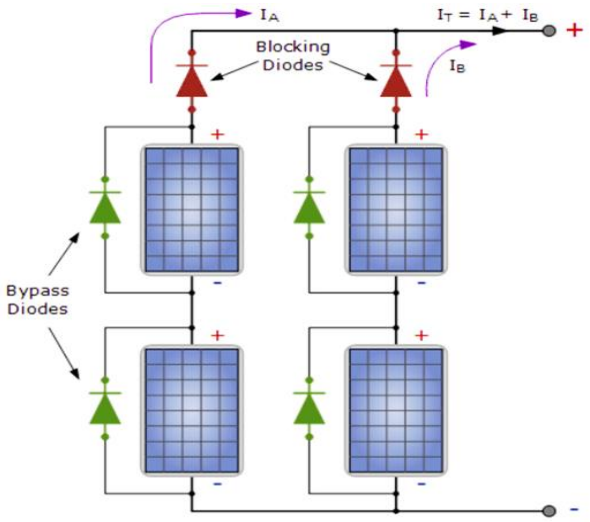

Figure 3.3: Bypass and blocking diodes in a PV system [51].

Figure 3.4 shows that the characteristics of an array with bypass diodes differ from the one without these diodes. Since the bypass diodes provide an alternate current path, cells of a module no longer carry the same current when they are partially shaded. Therefore, as shown in Figure 3.5 the power-voltage curve develops multiple maxima (global maxima which is the true MPP while others are local peaks). Unfortunately, presenting multiple maxima in the PV characteristic is a crucial issue and most of the conventional MPPT algorithms may not distinguish between the local and global maxima [50].

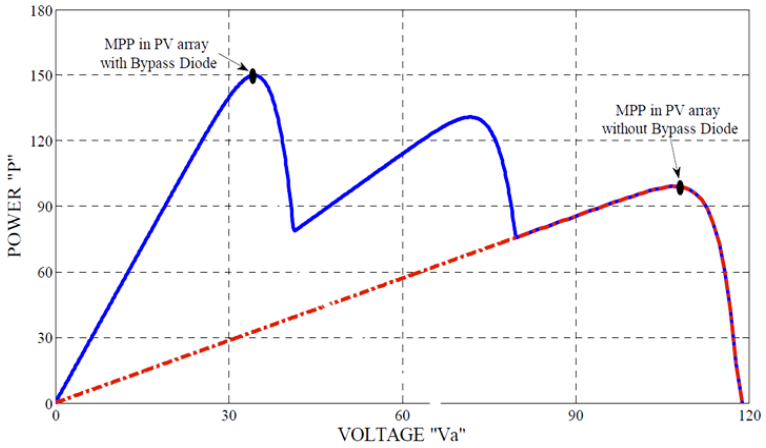

Figure 3.4: PV characteristic curves under partial shading with and without bypass diodes [50].

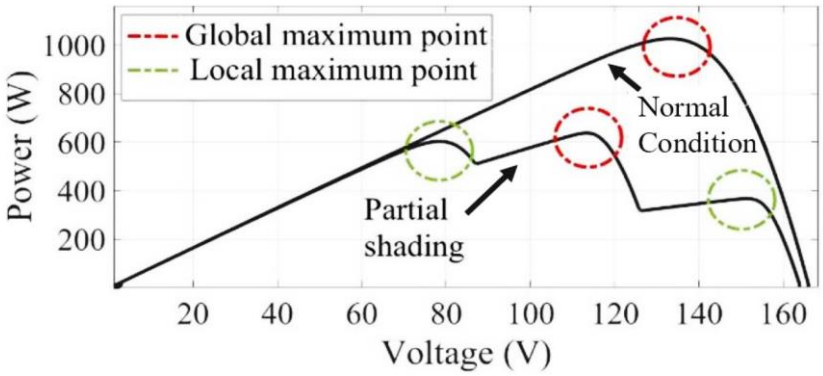

Figure 3.5: PV characteristic curves for uniform and non-uniform irradiations [52]

- **Blocking diodes**

These blocking diodes, also called a series diode or isolation diode, ensure that the electrical current only flows in one direction “OUT” of the series array to the external load, controller or batteries. The reason for this is to prevent the current generated by the other parallel connected PV panels in the same array flowing back through a weaker (shaded) network. However, as shown in Figure 3.3, when multiple solar panels are connected in parallel, blocking diodes should be used in each parallel connected branch [51].

3.2.2.1 Particle Swarm Optimization

Particle Swarm Optimization (PSO) algorithm is a multivariable optimization technique based on the bird flocking behavior model, which is simpler than other intelligent algorithms, with fast calculating speed and high accuracy, as presented in 1995.

The PSO algorithm defines initial position of a random particle swarm which are randomly distributed in the search space. After the algorithm starts, the particles update their velocity and position and find the optimal position iteratively. During iteration, each particle has a fitness value determined by an objective function, and a velocity which the particle uses to determine the flight direction and distance. Particles calculate the direction and velocity of the next iteration based on the best position found by the particle itself (P_{besti}), which is stored as individual best solution, and the best position in the swarm (G_{best}), which is stored as the best global solution. These two extreme values are constantly updated as each particle's velocity and position are updated, and eventually stabilizing at the global extreme point [53].

In every iteration pf the particle, the update formula of the velocity, position, P_{besti} and G_{besti} of each particle is [54]:

$$V_i^{k+1} = wV_i^k + c_1 r_1\left(P_{besti}^k - X_i^k\right) + c_2 r_2\left(G_{best}^k - X_i^k\right) \quad (3.1)$$

$$X_i^{k+1} = X_i^k + V_i^{k+1} \quad (3.2)$$

$$P_{besti} = \begin{cases} P_{besti} & f(X_i) \geq f(P_i) \\ X_i & f(X_i) < f(P_i) \end{cases} \quad (3.3)$$

$$G_{besti} = max\{f(P_{best0}); f(P_{best1}); \dots\dots; f(P_{bestm})\} \quad (3.4)$$

Where:

$$i = 1,2,3,\dots\dots,m.$$

m: is the number of particles.

X_i and V_i : are the position and velocity of particle i.

k: is the number of iterations.

w: is the particle inertia weight.

c_1 and c_2 : are learning factors.

r_1 and r_2 : are random numbers between (0,1).

The position of the particle is set to the operating voltage of the system and the speed of the particle is set to the system's voltage increment. The current optimal value of the particle is set to the maximum power point voltage of each particle in the system. The optimal solution of

the population is set to the maximum power point voltage of the system [55]. The flowchart of the PSO algorithm is shown in the figure below.

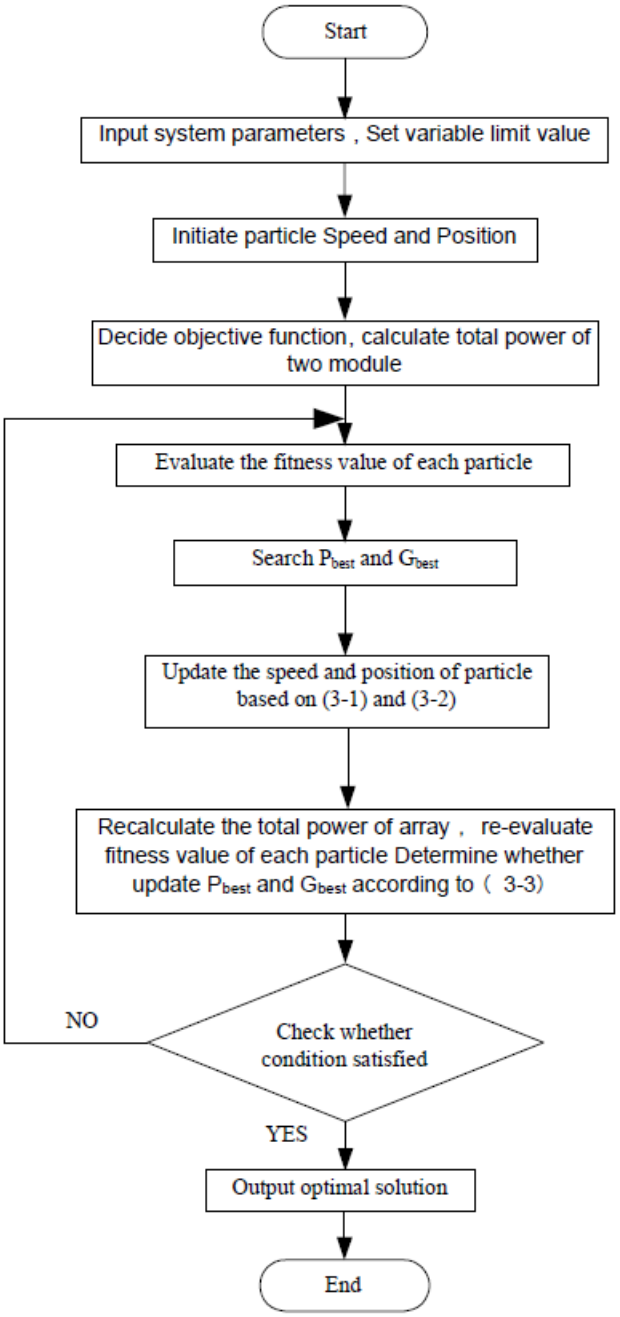

Figure 3.6 : Flowchart of MPPT control based on PSO algorithm [54].

3.2.2.2 Cuckoo Search Optimization algorithm

Cuckoo search (CS) is an evolutionary optimization algorithm that was inspired by Yang and Deb (2009) from species of bird called the Cuckoo. Cuckoos are fascinating birds, not only because of the beautiful sounds they can make, but also because of their aggressive reproduction strategy, by which mature cuckoos lay their eggs in the nests of other host birds or species [56]. It uses a technique to search for a suitable host nest where in it flies randomly from one nest to another, searching for the best nest chosen as the one with the highest chance of eggs being hatched safely. The cuckoos sometimes drop the eggs of the host bird out of the nest to increase the chances of their eggs hatching successfully. Some species of cuckoos can adapt the shape of their eggs to be similar to those of the host bird, in order to decrease the chance of discovery. If the host bird discovers the cuckoo's trick, it may throw out the cuckoo's eggs or abandon the nest [57].

- **Cuckoo Search methodology**

Cuckoo Search is basically based on three idealized important rules.

1. Each cuckoo lays one egg at a time and dumps its egg in a randomly chosen nest.
2. The best nest with high-quality eggs will carry over to the next generation.
3. The number of available hosts' nests is fixed, and the egg laid by a cuckoo is discovered by the host bird with a probability P_a such that: $0 \leq p_a \leq 1$.

Based on these three rules, the possibility is that the host bird can either throw the egg away or abandon the nest and build a completely new nest. For simplicity, this last assumption can be approximated by the fraction p_a of the n nests that are replaced by new nests (with new random solutions) [56].

- **Lévy flight**

Searching for a suitable host bird's nest is an important part of cuckoo's reproduction strategy. Normally, the search for the nest is similar to the search for food, which takes place in a random or in a quasi-random form. In general, while searching for food, animals choose directions or trajectories that can be modeled by certain mathematical functions. One of most common models is the Lévy flight. A Lévy flight is a random walk in which the step-lengths have a Lévy distribution, a probability distribution that is heavy-tailed. When defined as a walk in a space of dimension greater than one, the steps made are in isotropic random directions [58]. Such behavior is adopted in the meta-heuristic search algorithm for optimization problem. In CS, nest searching steps of cuckoo is also characterized by Lévy flight. Mathematically, a Lévy

flight is a random walk where step sizes are extracted from Lévy distribution according to a power law: $y = l^{-\lambda}$ [59]

Where l is the flight length and λ is the variance. Since $1 < \lambda < 3$, thus y has an infinite variance. The following Figure 3.7 depicts an example of Lévy flight in a two-dimensional plane. Due to the virtue of Lévy distribution, the steps consist of many small steps and occasionally large-step, long distance jumps. Comparing to other meta-heuristic algorithms, these long jumps may increase the search efficiency of cuckoo search significantly in some cases, especial for multimodal, nonlinear problems.

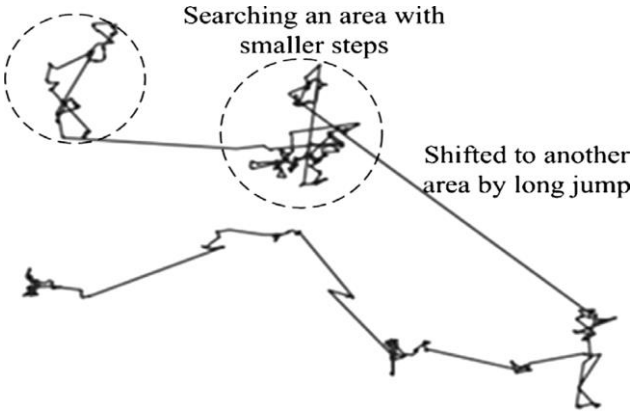

Figure 3.7: A Lévy flight in 2-dimensional plane.

When generating a new solution x^{t+1} for a cuckoo, a Lévy flight is performed as dictated by the following expression [59]:

$$x_i^{(t+1)} = x_i^{(t)} + \alpha \oplus \text{Lévy}(\lambda) \tag{3.5}$$

Where:

- $x_i^{(t+1)}$: New solution
- $x_i^{(t)}$: Current location (samples/eggs)
- i : sample number
- t : number of iteration
- $\alpha > 0$: step size
- $\oplus$: Entry wise multiplication
- λ : Levy exponent

$$\text{Lévy}(\lambda) \approx u = l^{-\lambda}, \quad (1 < \lambda < 3) \tag{3.6}$$

Based on the constraints imposed by the optimization problem, it is important to tune the value of a to get desired step size. In most cases a is used as:

$$\alpha = \alpha_0 \left(x_j^{(t)} - x_i^{(t)} \right) \tag{3.7}$$

Where α_0 is the initial step change.

- **MPPT for PV using CS**

To use CS for designing MPPT, appropriate variables have to be selected for the search. First are the samples; in this case, they are defined as the values of the PV voltages, i.e. Vi (i = 1, 2. . .n). The total number of samples is defined as *n*. Second, is the step size, denoted by a The fitness function (J) is the value of PV power at MPP. Since J is dependent on the PV voltage, thus J = f(V). Initially, the generated samples are applied to the PV modules and the power is set as the initial fitness value. The maximum power provided by its corresponding voltage is considered as the current best sample. Thereafter the Lévy flight is performed; consequently, new voltage samples are generated based on the following equation [59]:

$$V_i^{(t+1)} = V_i^{(t)} + \alpha \oplus \text{Lévy}(\lambda) \tag{3.8}$$

Where: $\alpha = \alpha_0(\mathcal{V}_{best} - \mathcal{V}_i)$. A simplified scheme of the Lévy distribution is presented in [21] as :

$$\text{S}=\alpha_0(\mathcal{V}_{best} - \mathcal{V}_i) \oplus \text{Lévy}(\lambda) \approx K \times \left(\frac{u}{(|\mathcal{V}|)^{\frac{1}{\beta}}} \right) (\mathcal{V}_{best} - \mathcal{V}_i) \tag{3.9}$$

Where :

- β = 1.5,
- *k* is the Lévy multiplying coefficient (chosen by the designer),
- ***u*** and ***v*** are determined from the normal distribution curves, i.e :

$$u = N(0, \sigma_u^2) \ , \ v = N(0, \sigma_v^2) \tag{3.10}$$

If Γ denotes the integral gamma function, then the variable σ_u and σ_v are defined as:

$$\sigma_u = \left(\frac{\Gamma(1+\beta) \times \sin(\pi \times \beta/2)}{\Gamma\left(\frac{1+\beta}{2}\right) \times \beta \times (2)^{\left(\frac{\beta-1}{2}\right)}} \right)^{\frac{1}{\beta}}, \ \sigma_v = 1 \tag{3.11}$$

The respective power for the new voltage samples is measured from the PV modules. By comparing the power values, the maximum power given by the voltage is selected as the new best sample. Besides this best sample, others are randomly destroyed with a probability of

p_a such process emulates the behavior of the host bird discovering the cuckoo's eggs and then destroying those. Then new random samples are generated to replace the destroyed ones.

Consequently, the powers for all samples are measured again and the current best is selected by evaluating J. The iteration continues until all the samples have reached the MPP[59]. Flowchart of CS MPPT is appeared in Figure 3.8.

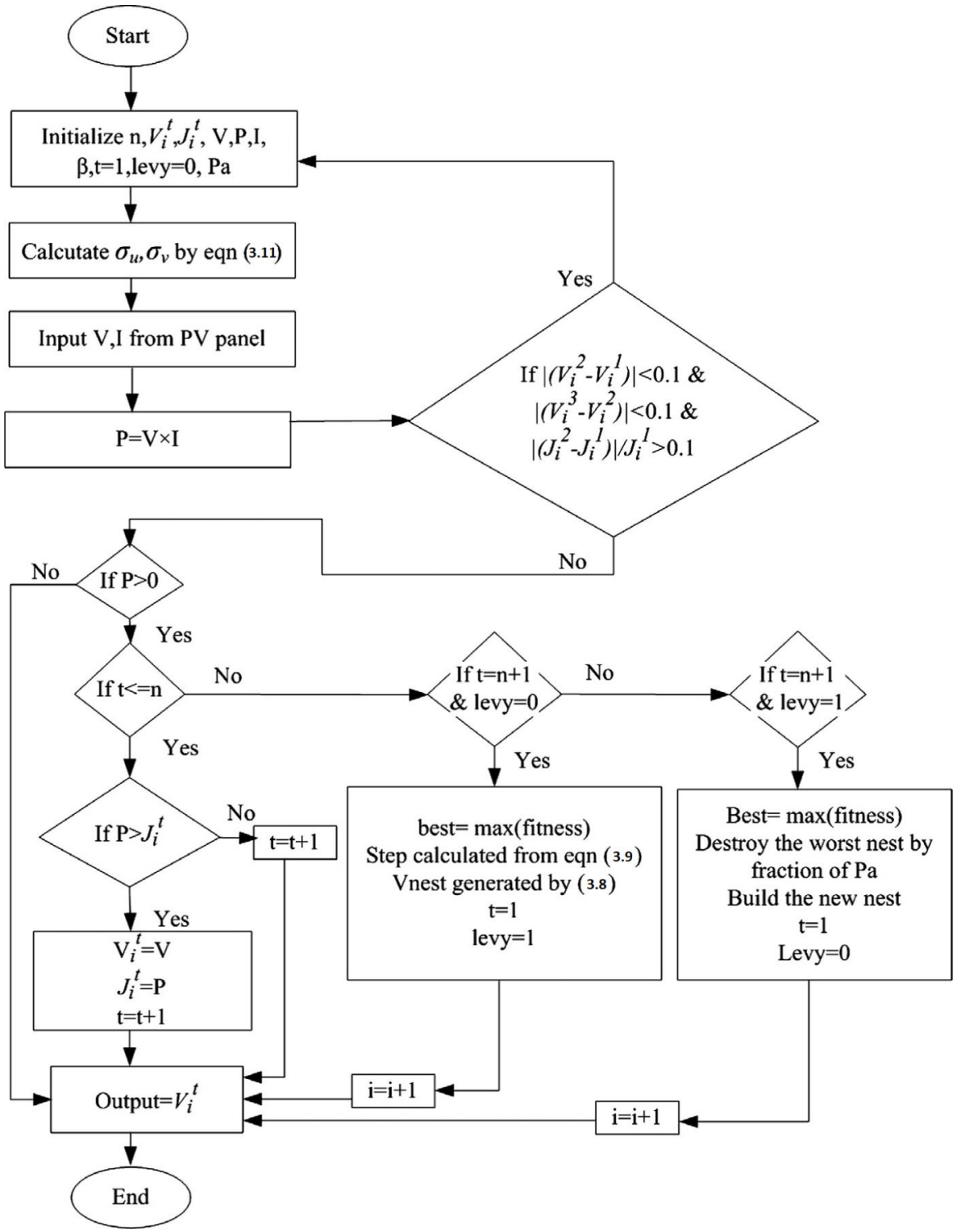

Figure 3.8: Flowchart for searching mechanism by CS.

3.3 Control of BLDC

A BLDC motor is a permanent magnet synchronous motor that uses position detectors and an inverter to control the armature currents. The BLDC motor is sometimes referred to as an inside-out dc motor because its armature is in the stator and the magnets are on the rotor and its operating characteristics resemble those of a DC motor [60]. Instead of using a mechanical commutator as in the conventional dc motor, the BLDC motor employs electronic commutation which makes it a virtually maintenance-free motor.

There are two main types of BLDC motors, trapezoidal and sinusoidal type. In the trapezoidal motor the back emf induced in the stator windings has a trapezoidal shape and its phases must be supplied with quasi-square currents for ripple free operation. The sinusoidal motor on the other hand has a sinusoidally shaped back emf and require sinusoidal phase currents for ripple-free operation. The shape of the back emf is determined by the shape of the rotor magnets and the stator winding distribution [61]. The trapezoidal motor is a more attractive alternative for most applications due to its simplicity, lower price and higher efficiency [60].

3.3.1 Types of BLDC control

To control a BLDC motor with the best efficiency, we have to know the rotor position at all times. To achieve this there are two modes. One is called the sensor mode, where the information read back from the motor is the one coming from Hall Effect sensors (1 per phase). The other one is the sensor less mode, where the Back Electromotive Force (BEMF) signal information is the one read back from the motor [62].

3.3.2 The Rotor Position Sensor

The present position of the rotor is required to determine the next commutation interval. In BLDC motors the commutation is done by electronic switches which need the rotor position. The appropriate stator windings have to be energized when rotor poles align with the stator winding. The BLDC motor can also be driven with predefined commutation interval but to achieve precise speed control and maximum generated torque, brushless commutation should be done with the knowledge of rotor position. In control methods using sensors, mechanical position sensors, such as a hall sensor, shaft encoder or resolver have been utilized in order to provide rotor position information. The hall effect sensor doesn’t provide information on precisely where the rotor is within a sector but instead it allows to detect the rotor transitions from one sector to another, and actually sector information is all we need to know when to

commutate the motor. In sensor less control BLDC motors can be commutated by monitoring the back EMF signals instead of the Hall sensors. Back EMF is proportional to the speed of rotation, at a very low speed, the back EMF would be at a very low amplitude to detect zero-crossing. The motor has to be started in open loop, from standstill and when sufficient back EMF is built to detect the zero-cross point, the control should be shifted to the back EMF sensing. The minimum speed at which back EMF can be sensed is calculated from the back EMF constant of the motor. With this method of commutation, the Hall sensors can be eliminated and, in some motors, the magnets for Hall sensors also can be eliminated. This simplifies the motor construction and reduces the cost as well [63]. In this work, we will use the sensor control type along with the Hall effect sensor.

A timing diagram showing the relationship between the sensor outputs and the required motor drive voltages is shown in the Figure 3.9 bellow:

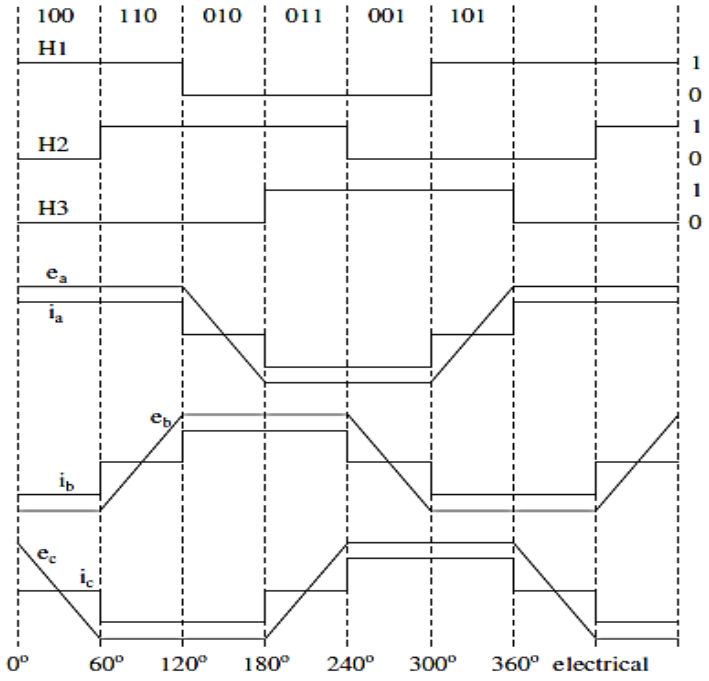

Figure 3.9: Ideal back emf's, phase currents, and position sensor signals

3.3.3 Commutation and BLDC Drive (VSI)

BLDC motors exist in many configurations but the three-phase motor is the most common type due to its efficiency and low torque ripple. Generally, three phase motor is fed with three phase three leg voltage source inverter for controlling it. Here the IGBT based VSI

which is presented in Figure 3.10, is used for feeding the BLDC motor with DC link charged by a converter**.**

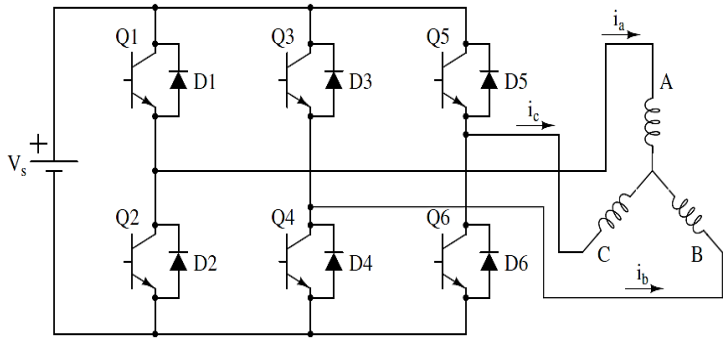

Figure 3.10: Simplified BLDC drive scheme LDC drive scheme

This topology provides two-way control of motor by controlling dc link voltage and by PWM control of inverter. The VSI is used here only to energize the proper phase of motor for fixed period, so that the torque produced by motor remains in one direction. For this purpose, the hall sensors are required which are mounted on motor. As the pole passes the sensor, the signal comes from motor which needs decoding for estimating the proper phase sequence activation which is represented in the table below [64]:

Table 3.1: Switching sequence.

Switching Interval	Seq. number	Pos. Sensors			Switch closed		Phase current		
		H1	H2	H3			A	B	C
0° - 60°	0	1	0	0	Q1	Q4	+	-	Off
60° - 120°	1	1	1	0	Q2	Q6	+	Off	-
120° - 180°	2	0	1	0	Q3	Q6	Off	+	-
180° - 240°	3	0	1	1	Q3	Q2	-	+	Off
240° - 300°	4	0	0	1	Q5	Q2	-	Off	+
300° - 360°	5	1	0	1	Q5	Q4	Off	-	+

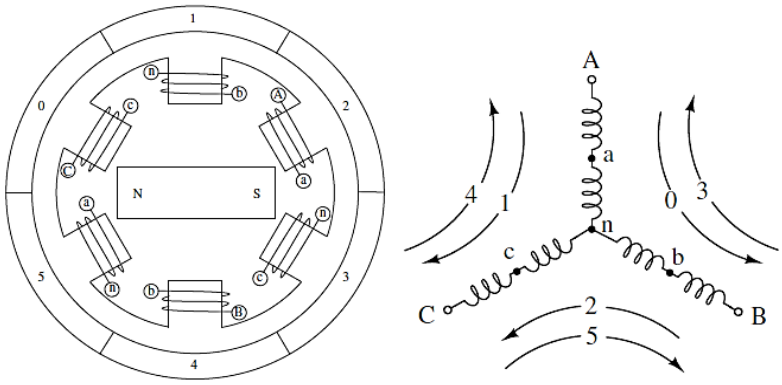

Figure 3.11: BLDC motor cross section and phase energizing sequence

This control is designed for commutation of the motor. As in case of brush DC motor, the commutation takes place at brushes where current reverses its direction. But due to absence of brushes in BLDC this commutation is carried out by proper phase switching of inverter and thus it is known as electronic commutation. The VSI requires a proper switching sequence for applying electronic commutation to the BLDC motor, so that a symmetrical current should flow from the DC link of VSI for $3\pi/2$ and should be placed symmetrically at the steady horizontal portion of trapezoidal back-EMFs for all three phases. To sense the rotor position of motor, the optical Hall Effect position sensors are placed on motor with span of 60°, to generate the electronic commutation pulses for VSI which feeds the BLDC motor.

As the switches, S1 and S2 of the inverter starts conducting, then a line current, I_{ac} starts flowing from DC link capacitor to the stator of motor, and its magnitude is decided by the DC link voltage (V_{DC}), back-EMF's (E_{an} and E_{bn}) , resistances (Ra and Rb) and the self-inductance and mutual inductance (La , Lb and Lm) of the stator windings.

The hall signals need decoding and passing through a truth table so that a proper sequence of switching is achieved. The truth table for switching is developed from all above-mentioned parameters so as to run motor in same direction [65].

3.3.4 BLDC Speed control using PWM technique

As discussed, BLDC motor means brushless DC motor as it does not have brushes for commutation so it is controlled by switching operation. The hall sensor inputs which give the position of the rotor is fed to the microcontroller. The microcontroller compares it with the reference speed and generates an error signal. The PWM module of the controller (PI) generates

appropriate PWM signals, which are applied to the three-phase inverter at the appropriate time to trigger the appropriate switches [66].

The PWM signal is basically a square wave signal that repeats itself at a certain frequency as presented in Figure 3.9.

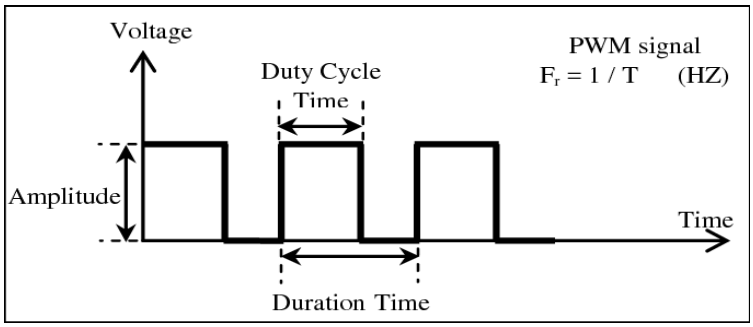

Figure 3.12: PWM signal

In PWM method, operating power to the motors is turned on and off to modulate the current to the motor. The ratio of on to off time is called as duty cycle. The duty cycle determines the speed of the motor. The desired speed can be obtained by changing the duty cycle. The Pulse Width Modulation (PWM) in microcontroller is used to control duty cycle of DC motor drive [63].

PWM technique is one of the most popular speed control techniques for BLDC motor. In this technique a high frequency chopper signal with specific duty cycle is multiplied by switching signals of VSI. Therefore, it is possible to adjust output voltage of inverter by controlling duty cycle of switching pulses of inverter [67]. The principle of generating PWM waveform is shown in Figures 3.10 and 3.11.

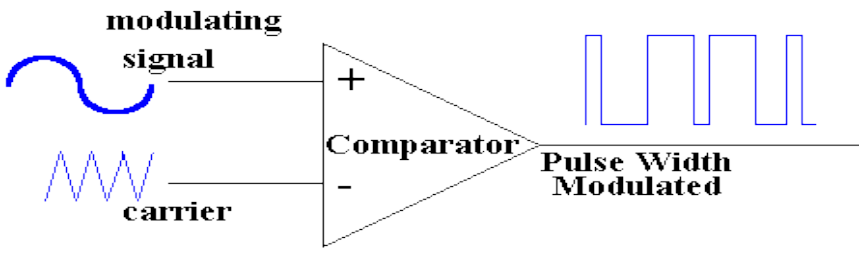

Figure 3.13: The principle of generating PWM

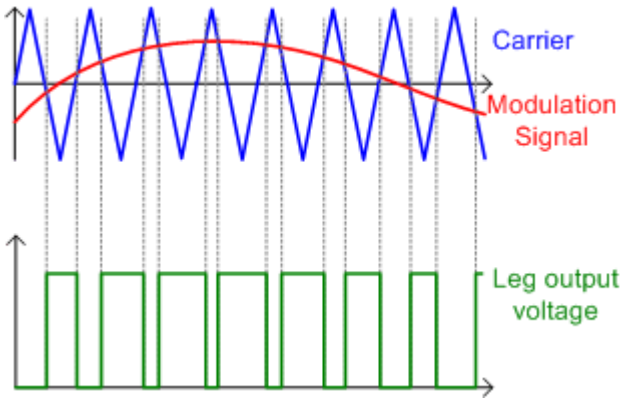

Figure 3.14: The carrier, modulation signal and PWM waveforms

Average output voltage is controlled through duty cycle of PWM. The relationship between average output voltage, duty cycle and input voltage is [63]:

$$Vavg = D\ Vinput$$

D = Duty cycle

$Vavg$ = Average output voltage

$Vinput$= Input DC voltage

The motor speed depends only on the amplitude of the applied voltage. This can be adjusted using PWM technique. The required speed is controlled by a speed controller. This is implemented as a conventional proportional-Integral controller. The difference between the actual and required speeds is given as input to the controller. Based on this data PI controller controls the duty cycle of the PWM pulses which correspond to the voltage amplitude required to maintain the desired speed. When using PWM outputs to control the six switches of the three-phase bridge, variation of the motor voltage can be achieved easily by changing the duty cycle of the PWM signal. In case of closed loop control the actual speed is measured and compared with the reference speed to find the error speed. This difference is supplied to the PI controller, which in turn gives the duty cycle PMBLDC motor is popular in applications where speed control is necessary and the current must be controlled to get desired torque. The basic structure for closed loop control of the PMBLDC motor drive is shown in the figure 10. It consists of an outer speed control loop, an inner current control loop for speed and current control respectively. Speed loop is relatively slower than the current loop [63].

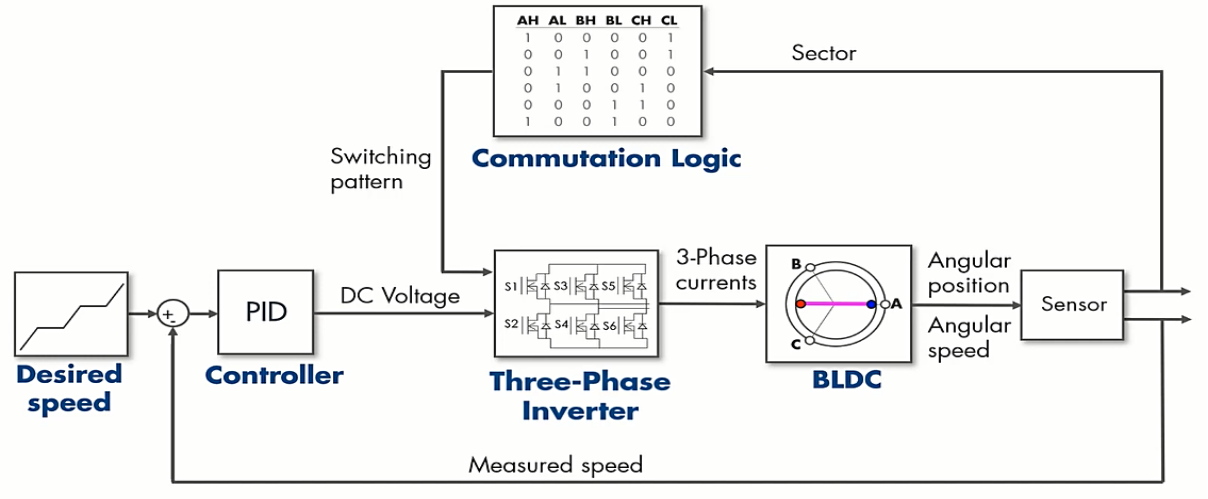

Figure 3.15: Closed loop control of the BLDC motor

3.3.5 BLDC Speed control using Hysteresis control

Hysteresis control is one of the simplest closed-loop control schemes. In hysteresis control, the value of the controlled variable is forced to stay within certain limits around its reference value. For example, to control motor speed, the motor is turned off if the speed reaches a certain level above the reference speed and turned back on when the speed falls below a certain level below the reference speed [69].

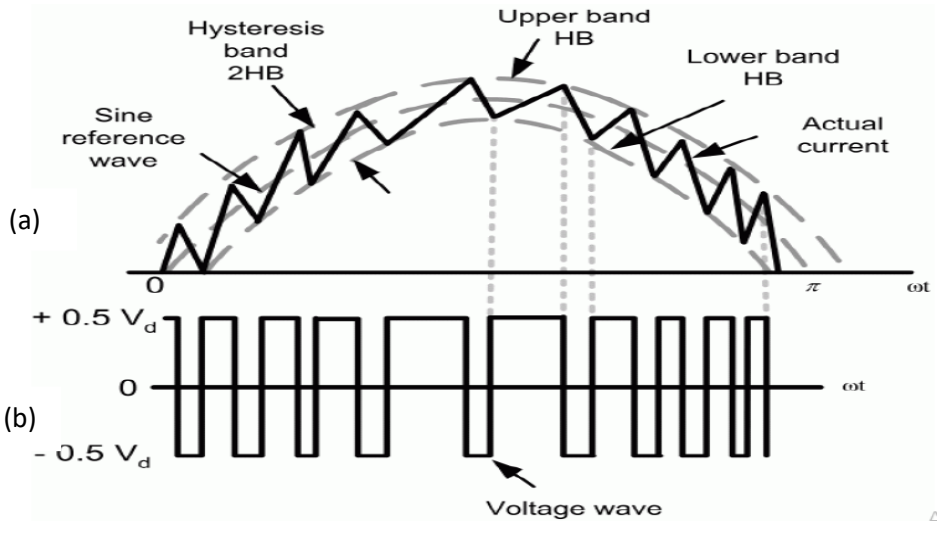

Figure 3.16: a) Hysteresis band, (b) pulses depending upon the actual current wave form

The control scheme adopted in this proposed technique is very simple. The current controller adopted is a hysteresis current controller. Upper and lower hysteresis band is created by adding and subtracting a band ‘h’ with the reference signal respectively shown in the

Figure 3.16 (a) & (b). The change in speed is forced to fall within the hysteresis band. When the current goes above the upper hysteresis band ($+V_d$), the pulse is removed. This results in the current forced to fall as the current will flow and achieves the operating point. When the current goes below the lower hysteresis band ($-V_d$) the pulse is given to the switch, so the current increases linearly. In this way the switching of the power switch can be done to track the reference speed command & the resultant current drawn by inverter, and maintains improved speed regulation & torque ripple minimization [70].

A block diagram of the BLDC motor drive system using the hysteresis control is shown in figure 3.17:

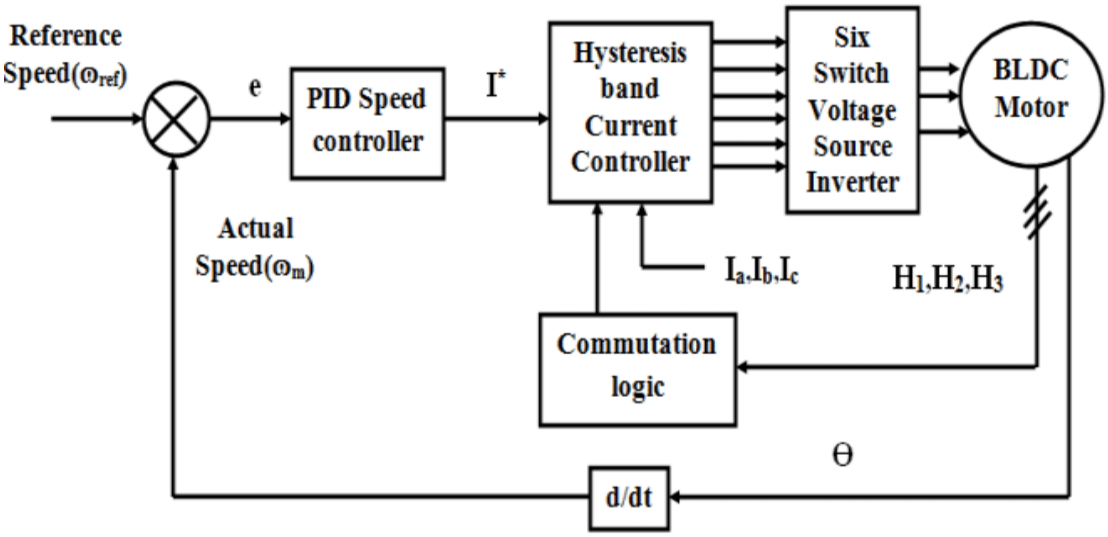

Figure 3.17: block diagram of the BLDC motor drive system

3.4 Conclusion

In this chapter the conventional MPPT algorithm P&O was set in normal weather conditions. Whereas, the PSO and CS algorithms were proposed to track the MPP under partial shading conditions. Furthermore, the selection of the BLDC motor to drive the centrifugal pump is justified by its high efficiency and low maintenance. In addition, the different control techniques of this motor are presented.

CHAPTER 4

SIMULATION AND RESULTS

4.1 Introduction

This chapter describes how the SIMULINK model of the proposed solar water pumping system was implemented to test and verify its functionality under various conditions. First, the PV system is tested to extract the characteristics mentioned in Chapter 2 in both normal and shaded conditions. Next, the performance of the SWPS is tested under variable irradiance describing the system designed with a closed loop controller as well as the open loop system. In the shaded conditions, the performance of the P&O and Cuckoo algorithms is tested.

4.2 PV array characteristics

To simulate the PV system described in chapter three, a Trina Solar TSM-250PA05.08 PV model was used. Specifications of the chosen module are shown in Figure 4.1.

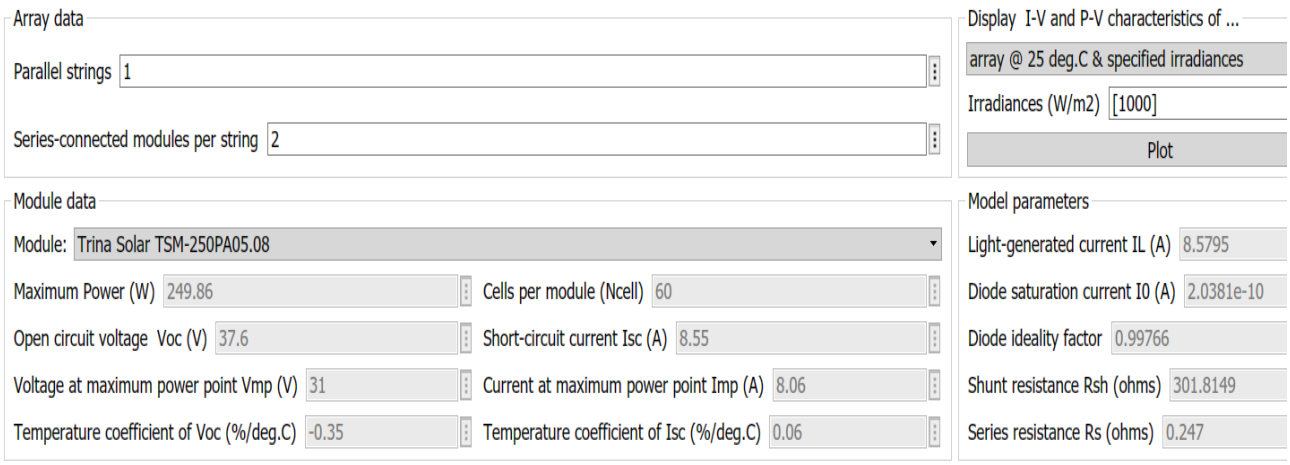

Figure 4.1: PV module specifications

4.2.1 Under normal conditions

Figure 4.2 and 4.3 show the model of five PV modules connected in series and its corresponding I-V and P-V characteristics curves.

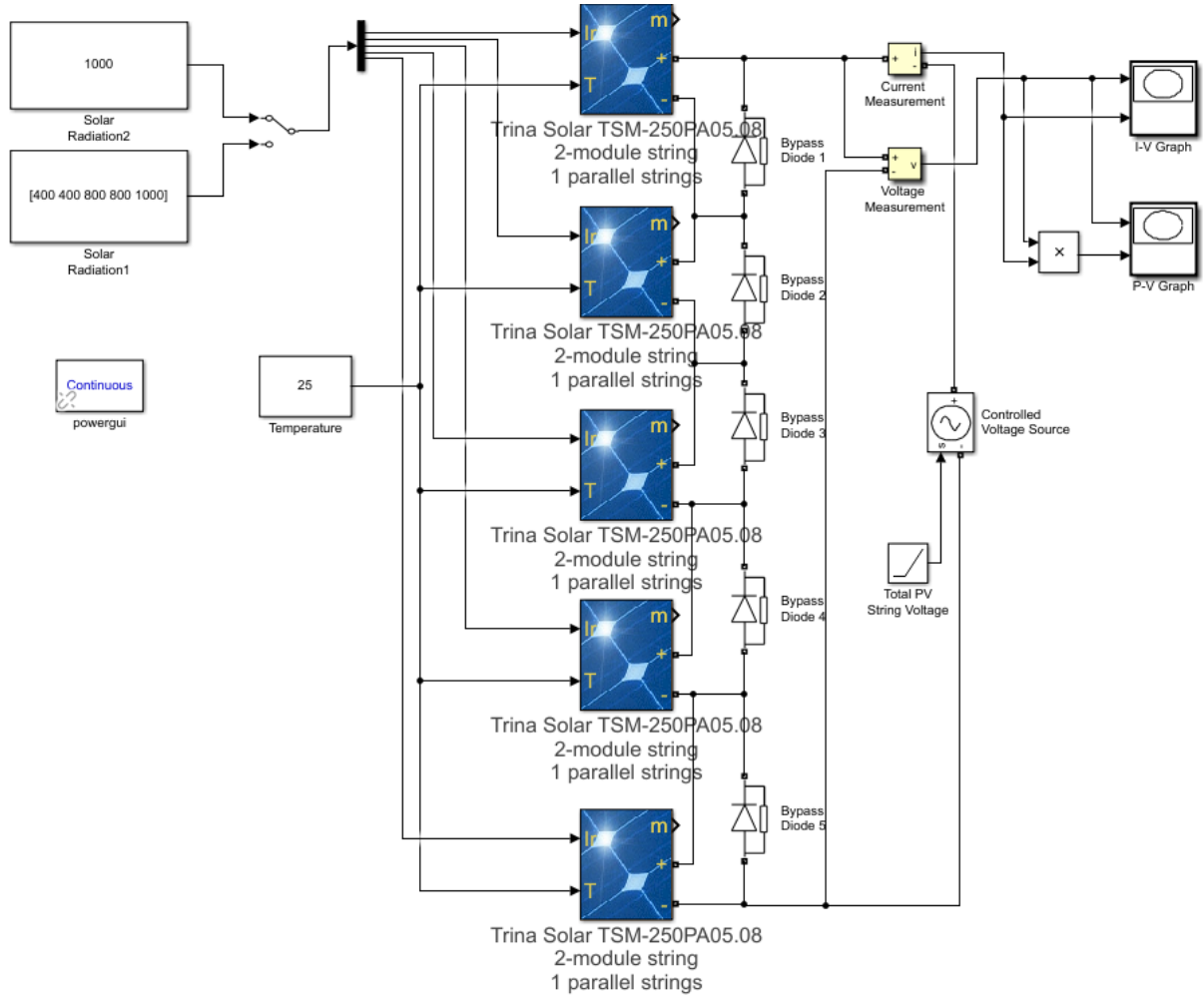

Figure 4.2: SIMULINK model of five PV modules in series under uniform conditions

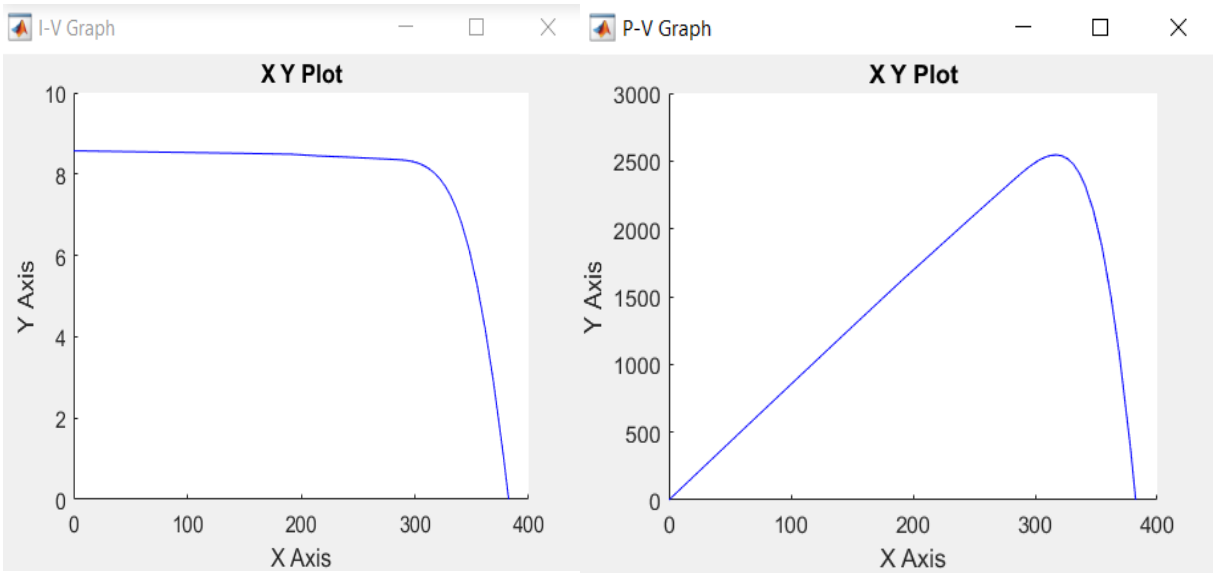

(a) (b)

Figure 4.3 : a- I-V and b- P-V characteristics of five PV modules in series under uniform conditions.

As can be seen from the simulation results , when the solar insolation is uniform, the P-V curve has an individual MPP.

4.2.2 Under partial shading conditions

To show the effect of the non-uniform solar irradiance on the PV characteristic of the PV modules, the model shown in Figure 4.4 was simulated.

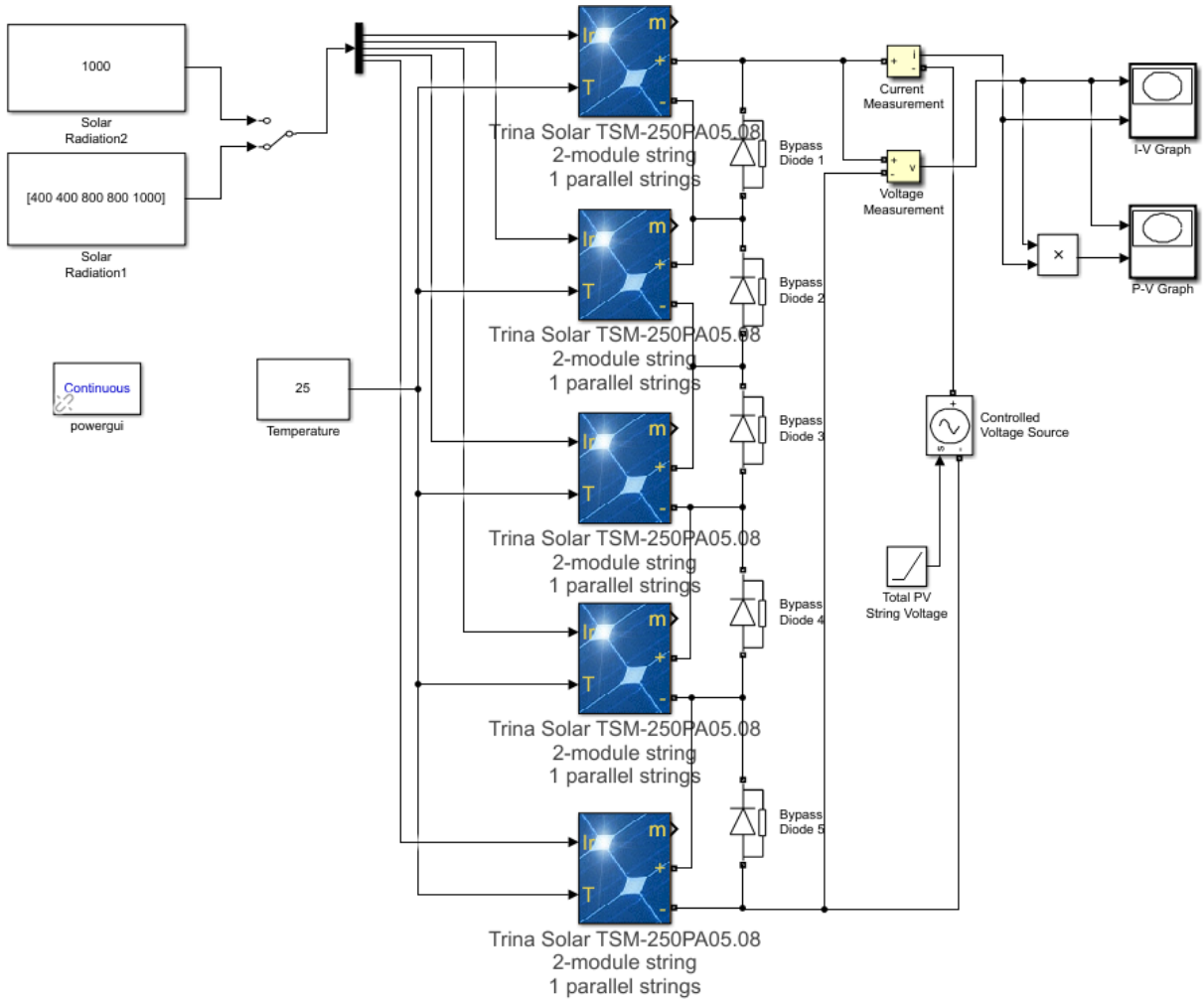

Figure 4.4: SIMULINK model of five PV modules in series under non-uniform conditions.

The P-V characteristic curve shown in Figure 4.5 develops multiple maxima when the PV modules are partially shaded due to bypass diodes effect.

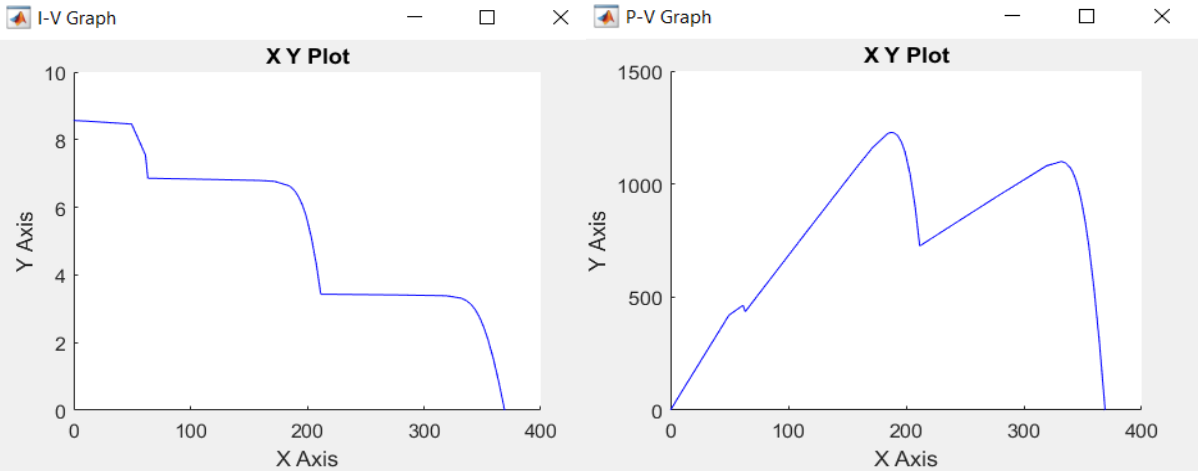

(a) (b)

Figure 4.5: (a) I-V and (b) P-V characteristic curves of PV modules under partial shading.

When the PV receives non-uniform insolation and the partial shading takes place, the curve will be more complicated. As the P-V characteristic suffers from many peaks, which contains only one MPP.

4.3 Simulation of the SWPS

The proposed water pumping system is simulated in MATLAB/Simulink under various conditions (variable irradiance and partial shading) and the simulation results of both cases are presented in the following sections :

4.3.1 Under variable irradiance

The proposed water pumping system is modeled and its performance is simulated in MATLAB/Simulink under various conditions using the conventional P&O. In order to study the performance of the algorithms under climate changing conditions, the irradiance signal was set as shown in figure 4.6.

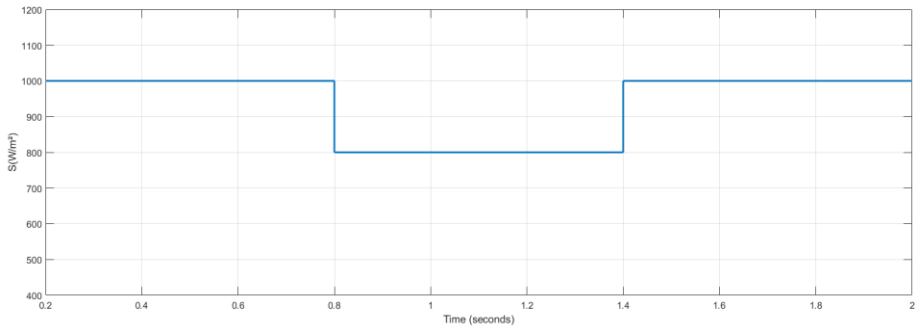

Figure 4.6: Irradiance profile

A. Dynamic Performances at open loop system

Figures 4.7 and 4.8 demonstrate that the system exhibits an excellent dynamic operation under the varying irradiance condition. Following sub-sections demonstrate the performances of the solar PV array and the motor-pump. The steady state and starting responses of the BLDC motor pump and PV array, are shown in the figures bellow and described in the following sub-sections :

1) Solar PV Array Performance

As shown in figure 4.6, the irradiance level is reduced from 1000 W/m2 to 800 W/m2 and increased back to 1000 W/m2. The PV array power is optimized successfully under the considered dynamics and the MPP is directly achieved despite the sudden variation of solar irradiance level.

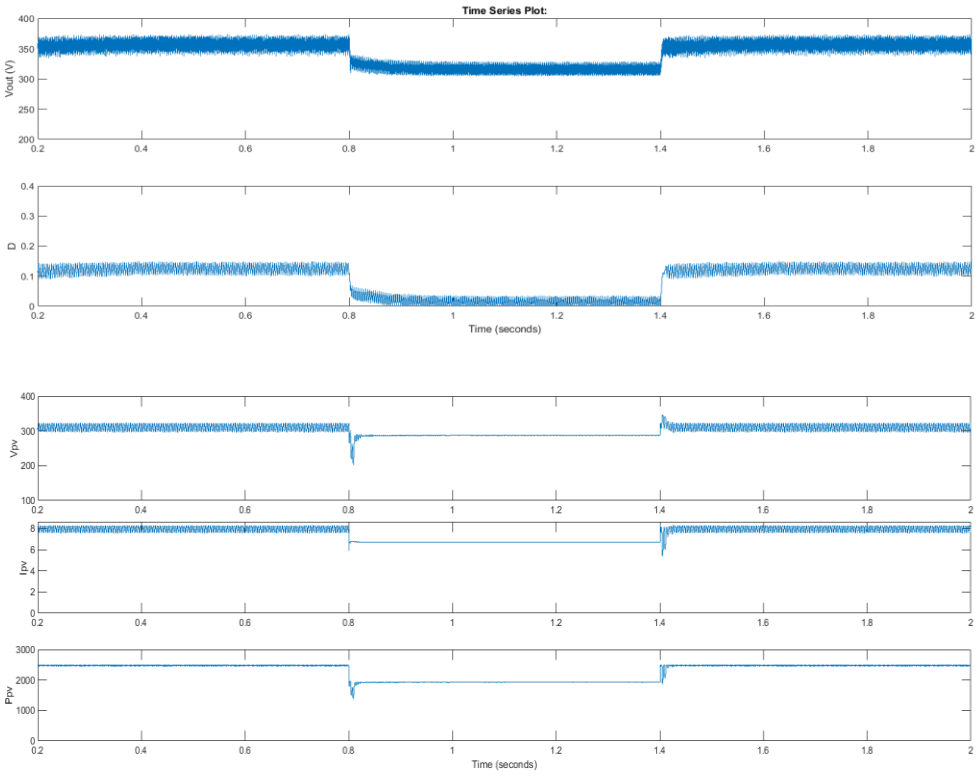

Figure 4.7: Dynamic performance of the PV array of the proposed water pumping system under variable irradiance

2) Brushless DC Motor-Pump Performance

Any variation in the atmospheric condition is strictly followed by the motor indices, as shown in figure 4.8. A smooth dynamic performance of the motor is preserved. The motor is governed by the PV array power, and adjusted through the optimum duty ratio by controlling the motor input voltage.

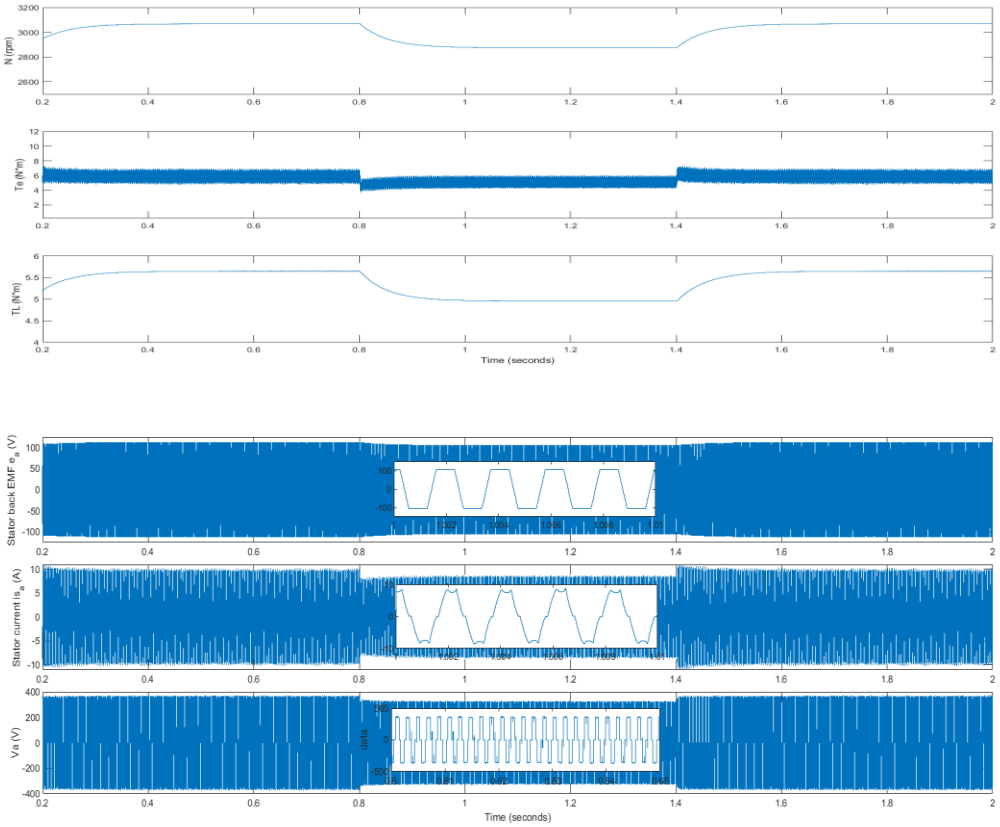

Figure 4.8: Dynamic performance of the BLDC water of the proposed water pumping system under variable irradiance.

B. Steady State and Starting Performances at closed loop

1) Solar PV Array Performance:

As seen in Figure 4.9, the obtained results are quite similar to the previous section with a slight increase in the duty cycle hence in the output voltage. The system still exhibits an excellent dynamic operation under the varying irradiance condition.

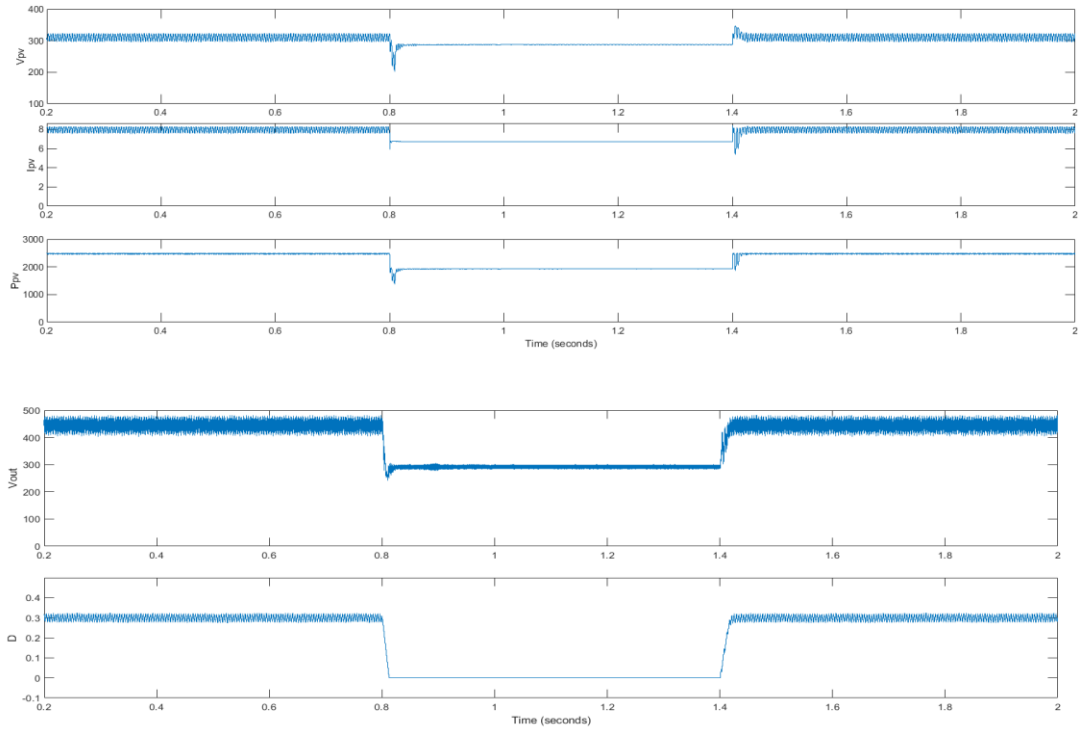

Figure 4.9: Dynamic performance of the PV array of the proposed water pumping system under variable irradiance

2) Brushless DC Motor-Pump Performance

Any variation in the atmospheric condition does not affect the motor indices, as shown in figure 4.8. A smooth performance of the motor is preserved, where the speed, induced torque and the load torque remain unchanged and unaffected by the variation of the irradiance.

After the irradiance drops to 800 W/m² at 0.8 seconds, the rotor speed in the closed loop system returns to its reference speed which is 2500rpm in a short time, this is due to the error compensation by the PI controller. Hence, for any variation or disturbance that affects the speed, the speed will be regulated so that the motor gets back to the desired speed.

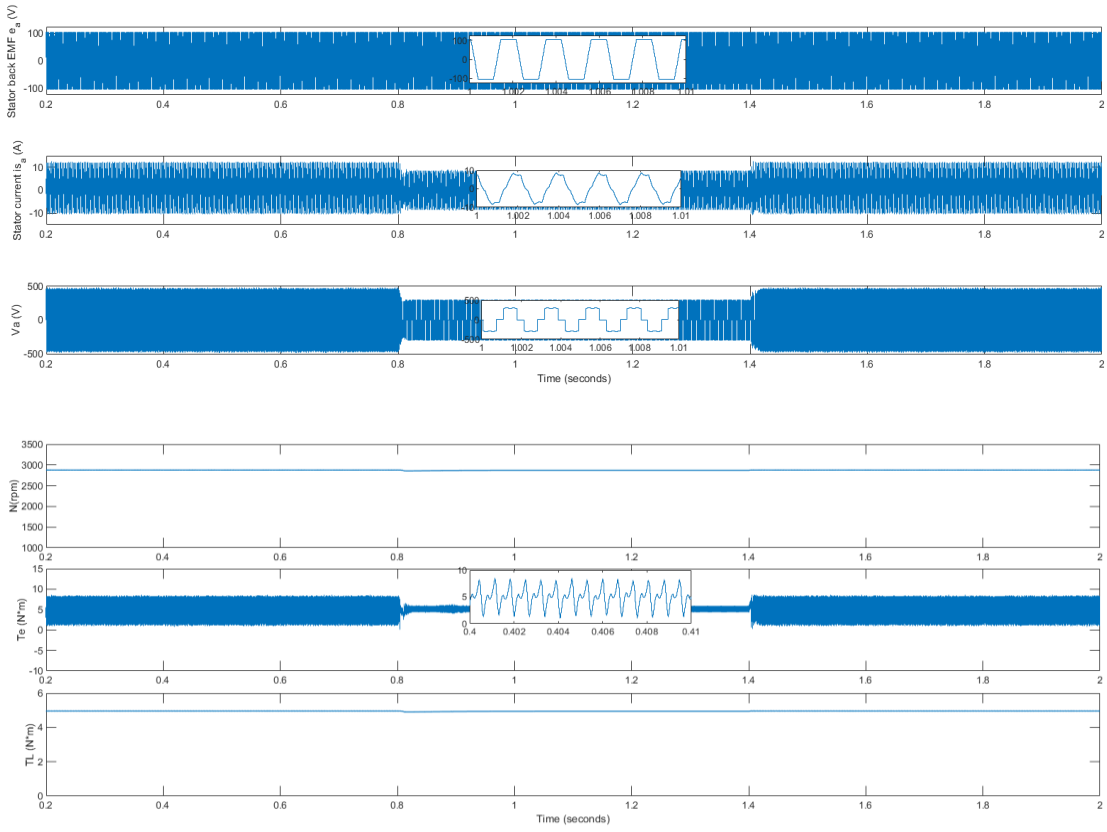

Figure 4.10: Dynamic performance of the BLDC motor of the proposed water pumping system under variable irradiance

4.3.2 Under shaded conditions

In reality, the output power of a photovoltaic cell is mainly influenced by ambient temperature and solar irradiation, although the change in ambient temperature has a small influence on the PV cell and it is not directly related to the speed of dynamic response. Therefore, the cell working temperature was fixed at 25°C in all simulations. However, in practice the irradiance is not always constant because of climate changing and partial shading phenomenon which leads to a sudden change in the PV panel output power. Consequently, the algorithm had to be tested under different irradiation levels to verify the speed of tracking.

The PV array was expected to produce 2500W with MPPT voltage and current of 310V and 8.5 A respectively at 1000W/m² solar irradiance.

In order to study the performance of the P&O and Cuckoo algorithms under partial shading phenomenon, the five PV modules were set to constant temperature (25°C) and different irradiance [400 400 800 800 1000].

A. Steady State and Starting Performances using P&O

The conventional Perturb and Observe algorithm which was introduced in chapter three was written as M-file code based on its algorithm in embedded MATLAB function.

The simulation results showed a good performance in tracking the maximum power point under variable irradiance.The simulation of the model under shaded condition, gives the results waveforms shown in Figures 4.11 and 4.12.

1) Solar PV Array Performance

As seen from the results the simulated P&O algorithm failed to track the global MPP, it converged to the third peak of figure 4.5 the output power from the PV array is reduced.

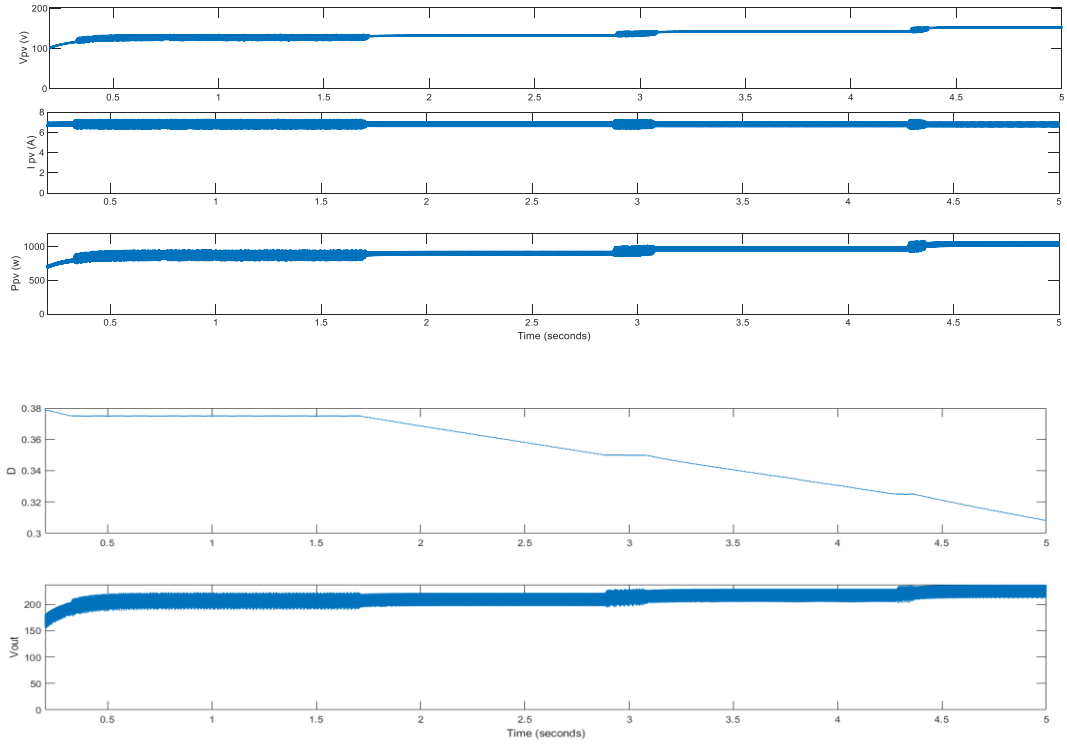

Figure 4.11: Dynamic performance of the PV of the proposed water pumping system under shaded conditions using P&O

2) Brushless DC Motor-Pump Performance

Under partial shading conditions, the output power from the PV array is reduced. Nevertheless, the motor-pump is able to deliver the water with the set PV array, operating at an MPP. The responses of PV array and BLDC motor -pump under such condition are presented in Figure 4.12. The BLDC motor-pump responds properly as per the available power from the PV array. Being a high efficiency motor, the BLDC motor offers a good amount of water delivery even at low input power.

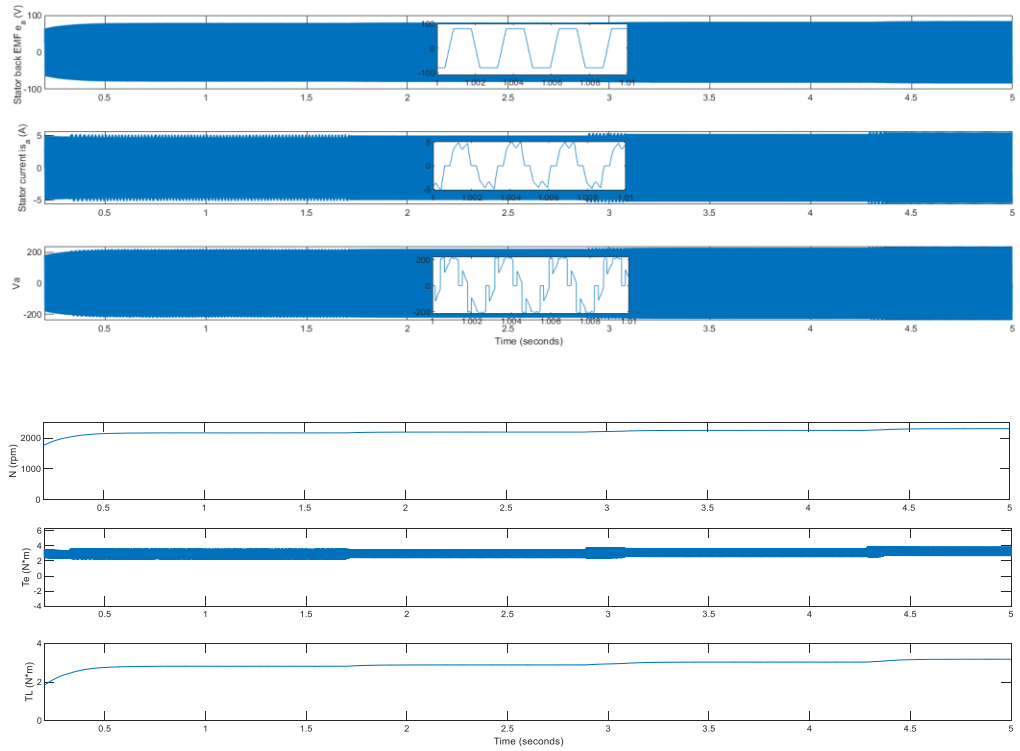

Figure 4.12: Dynamic performance of the BLDC motor of the proposed water pumping system under shaded conditions using P&O

B. Steady State and Starting Performances using Cuckoo

In this part P&O was replaced by Cuckoo algorithm. It was simulated under partial shading conditions and the results of simulation are given in the figures 4.13 and 4.14.

1) Solar PV Array Performance

The Cuckoo method captured the global peak effectively avoiding the local maximums under partial shading condition, which means a maximum extraction of the PV power. Comparing to P&O which tracked a local peak, the CS exhibits faster convergence speed, less oscillation around the MPP under steady-state conditions, and no divergence from the MPP during varying weather conditions.

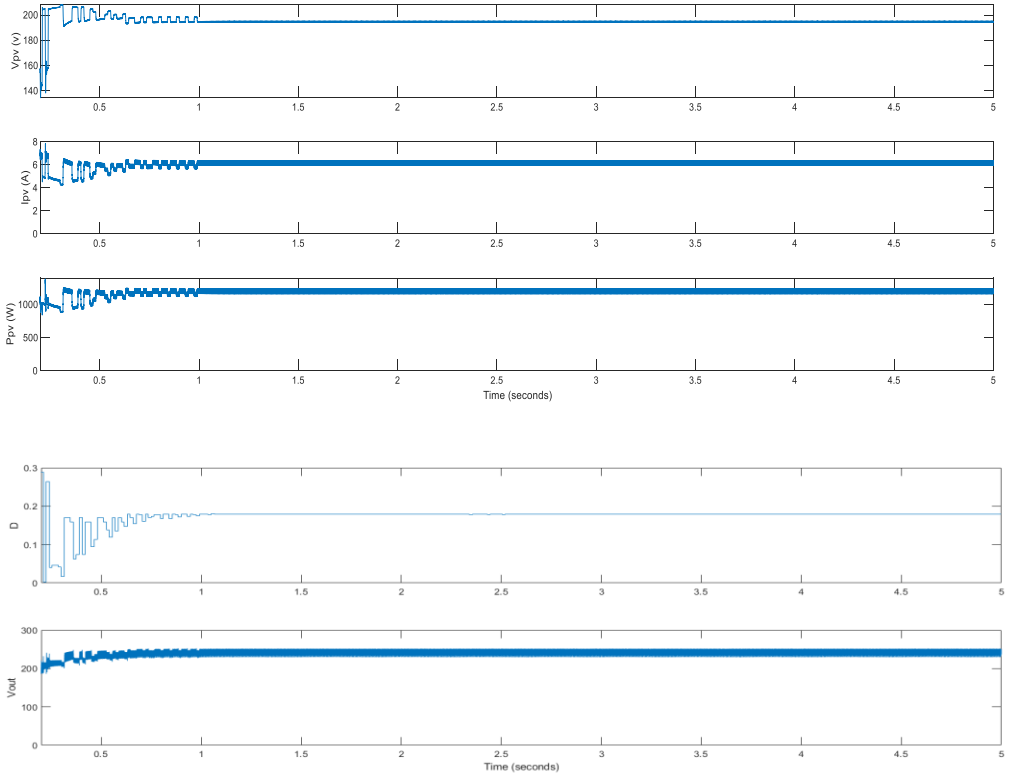

Figure 4.13: Dynamic performance of the PV of the proposed water pumping system under-shaded conditions using Cuckoo search

2) Brushless DC Motor-Pump Performance

Under partial shading conditions, the output power from the PV array is reduced. However, the BLDC motor shows a better performance when using CS algorithm since it runs on the maximum possible power as the CS tracks the MPP of the PV array as shown in Figure 4.13.

Practical results found in Figure 4.14 interpret the safe starting of BLDC motor under partial shading conditions.

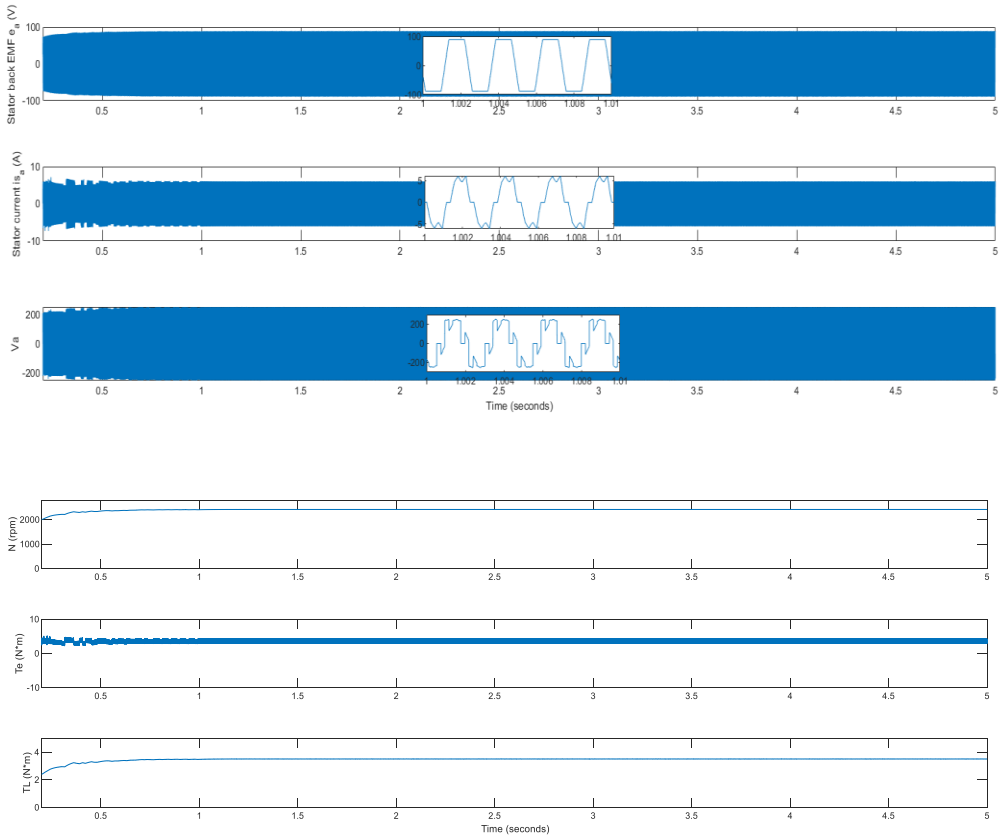

Figure 4.14: Dynamic performance of the BLDC motor of the proposed water pumping system under shaded conditions using Cuckoo search.

Table 4.1 : The power and speed values under different conditions.

	MPPT technique	Power(w)	Speed (rpm)	Control
Normal conditions	P&O	2500	3100	Open loop
		2500	2880	Closed loop
Shaded conditions	P&O	800	2100	Open loop
	Cuckoo	1250	2500	

4.4 Conclusion

In this chapter, CS algorithm has been used as an MPPT technique of partially shaded PV systems to avoid the limitations of the traditional technique P&O. The results demonstrate that CS performs better than P&O in terms of convergence speed, transient fluctuations and steady state performance under partial shading conditions which makes the energy loss at steady state almost zero. Although, under normal conditions the results proved that the P&O performs better. Finally, the simulated results demonstrate the worthiness of the proposed system.

General Conclusion:

Photovoltaic (PV) energy represents a promising and motivating renewable energy technology for future electricity generation and recently acquired worldwide attention. In addition, the advantages of PV power, such as no fuel costs, no air pollution, and noiseless, have boosted the demand of this type of energy in many applications such as water pumping systems.

In this thesis, a BLDC motor driven water pumping system based on PV generation was designed. The photovoltaic generator is a set of PV panels and their connection was chosen according to the power requirement of the associated power electronic converters, motor and the centrifugal pump. However, the power generated from such systems does not depend only on the climatic conditions, but also highly on the applied control technique. The maximum generated power from PV changes according to solar radiation and surrounding temperature change. Therefore, MPPT control techniques were used in order to improve the total system efficiency and extract the maximum PV energy over different operating conditions.

Furthermore, this system was simulated and tested using P&O and Cuckoo MPPT techniques in SIMULINK/MATLab. The performance of the two algorithms were compared under changing irradiation levels and partial shading condition. The simulation results showed that the P&O technique is more efficient compared to the CS technique under uniform irradiation. Whereas, under non-uniform irradiation the P&O failed to track the global MPP while the Cuckoo did successfully. Also, the dynamic characteristics of the BLDC motor such as speed, current, torque and back EMF were analyzed. Simulation results show an improved performance of the BLDC under various irradiance conditions when the proposed Cuckoo technique is used.

Future Work:

The following future research works is suggested as an extension to the knowledge presented in this thesis:

- Experimental implementation of the proposed SWPS.
- The extension of the proposed system to a hybrid system such as Diesel-PV system.
- Application of enhanced MPPTs based on metaheuristic method to improve the stability and the tracking capability under different conditions.
- Techno-economical study of the proposed system.

Appendix

Table A.1: BLDC motor parameters

Design Parameters	Value
Rated Torque T_d	4.2 Nm
Rated Power P_d	1.5 kW
Rated Speed N_r	2880rpm
Poles N_m	10
Phase Resistance R_{ph}	0.7 Ω
Phase inductance L_{ph}	4mH
Torque constant K_t	0.7 N_m/A
Moment of Inertia J	0.0028 kg/m^3

Table A.2 Boost parameters

Element	Rating
Input capacitor C_1	2.34 e-5 F
Inductor	0.023 H
Output capacitor C_2	2.34 e-5 F

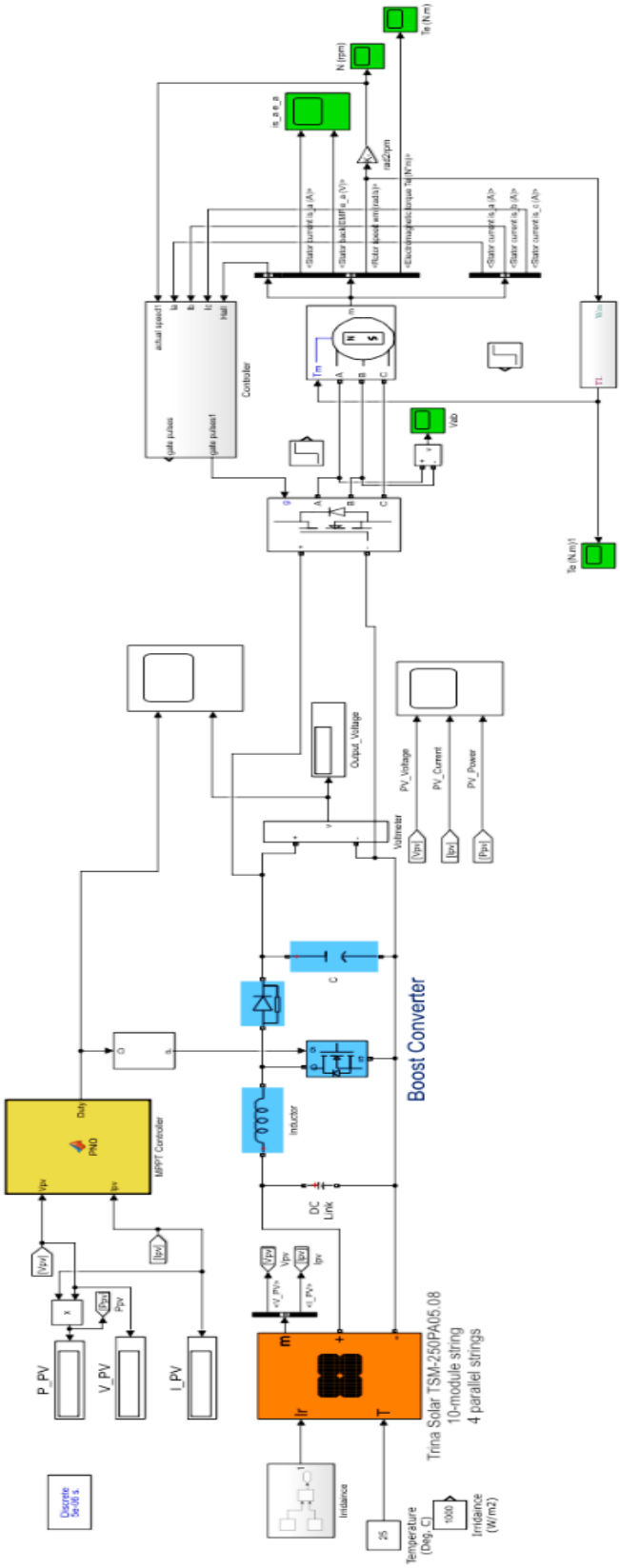

Figure A.1: Global scheme of the simulated system.

[1] Fathi A O Aashoor. Maximum power point tracking techniques for photovoltaic water pumping system, thesis submitted for the degree of Doctor of Philosophy, University of Bath, May 2015.

[2] DJERIOU. Salim. Performance Improvement of Photovoltaic Pumping System, thesis submitted for the degree of Doctor of Philosophy, University of M'hamed Bougerra,2018.

[3] Li, G.Q., Jin, Y., Akram, M.W. and Chen, X. (2017) Research and Current Status of

the Solar Photovoltaic Water Pumping System—A Review. Renewable and Sustainable

Energy Reviews, 79, 440-458. https://doi.org/10.1016/j.rser.2017.05.055

[4] Chandel, S.S., Naik, M.N. and Chandel, R. (2015) Review of Solar Photovoltaic Water

Pumping System Technology for Irrigation and Community Drinking Water

Supplies. Renewable and Sustainable Energy Reviews, 49, 1084-1099.

https://doi.org/10.1016/j.rser.2015.04.083

[5] J. Goldemberg and T. B. Johansson (2004) "World energy assessment overview: 2004 update," United Nations Development Programme, New York [Online]. Available: www.undp.org/energy/weaover2004.htm Global Status Report. [Online]. Available: http://www.ren21.net/.

[6] REN21, Paris, France: " Renewables 2017: GSR full report" 2017.(online). Available: www.ren21.net

[7] " Renewables 2019: GSR full report" 2019.(online). Available: www.ren21.net status, future prospects and their enabling technology. Renew. Sustain. Energy Rev.39,748–764.

[8] Talbi Billel . Contribution to Improvement in Control of a Photovoltaic Pumping System Maximum power point tracking techniques for photovoltaic water pumping system, thesis submitted for the degree of Doctor of Philosophy, University of Sétif 1, May 2018.

[9] V. Karthikeyan, S. Rajasekar, Vipin Das, P. Karuppanan and Asheesh Kumar Singh / Grid-Connected and Off-Grid Solar Photovoltaic System

[10] Vimal Chand Sontake , Vilas R. Kalamkar. Solar photovoltaic water pumping system - A comprehensive review. Department of Mechanical Engineering ,St.Vincent Pallotti College of Engineering & Technology , Nagpur 441108,India

[11] Stefan Siepman ,https://www.un-igrac.org/stories/solar-powered-groundwater-pumping

[12] Solar photovoltaic water pumping system A comprehensive review Vimal Chand Sontake a,n, VilasR.Kalamkar Department of Mechanical Engineering ,St. Vincent Pallotti College of Engineering & Technology , Nagpur441108,India Department of Mechanical Engineering ,Visvesvaraya National Institute of Technology, Nagpur440010, India.

[13] Design and control of a standalone PV water pumping systemEssam E. Aboul Zahaba, Aziza M. Zakib, Mohamed M. El-sotouhyb,∗*Department of Electrical Power and Machines, Faculty of Engineering, Cairo University, Giza, Egypt*b*Department of Power Electronics and*

*Energy Conversion, Electronics Research Institute, Dokki, Giza, Egypt*Received 5 October 2015; received in revised form 22 February 2016; accepted 6 March 2016.

[14] S.G. Malla, C.N. Bhende and S. Mishra, Photovoltaic based Water Pumping System, Indian Institute of Technology Bhubaneswar, 978-1-4673-0136-7/11/$26.00 ©2011 IEEE

[15] SOLAR WATER PUMPING SYSTEMS DESIGN, SELECTION AND INSTALLATION GUIDELINES / Guideline of The Pacific Power Association (PPA).

Can be found at : https://watermission.org/wp-content/uploads/2019/10/System-Design-Selection-and-Installation-Guidelines.pdf.

[16] "What is the history of solar energy and when were solar panels invented ?".In: (2015). url: https://news.energysage.com/the-history-and-invention-of- solar-panel-technology/.

[17] Villalva, M.G., Gazoli, J.R., Filho, E.R., 2009. Comprehensive approach to modeling and simulation of photovoltaic arrays. IEEE Trans. Power Electron. 24, 1198– 1208.

[18] A. S. "Sedra and K. C. Smith, Microelectronic Circuits". London, U.K.Oxford Univ. Press, 2006.

[19] Francisco M. González-Longatt. Model of Photovoltaic Module in Matlab.

[20] Rekioua, D., Matagne, E., 2012. Optimization of Photovoltaic Power Systems. Springer Verlag.

[21] Farivar, G., Asaei, B., 2011. A new approach for solar module temperature estimation using the simple diode model. IEEE Trans. Energy Convers. 26, 1118–1126.

[22] Bishop, J.W., 1988. Computer simulation of the effects of electrical mismatches in photovoltaic cell interconnection circuits. Solar Cells 25, 73–89.

[23] Kassis, A., Saad, M., 2010. Analysis of multi-crystalline silicon solar cells at low illumination levels using a modified two-diode model. Solar Energy Materials and Solar Cells 94, 2108–2112.

[24] Weidong Xiao, Dunford, W.G and Capel, A (n, d). A Novel Modeling Method for Photovoltaic Cells. 2004 35th Annual IEEE Power Electronics Specialists Conference.

[25] Villalva, M.G., Gazoli, J.R., Filho, E.R., 2009. Comprehensive approach to modeling and simulation of photovoltaic arrays. IEEE Trans. Power Electron. 24, 1198– 1208.

[26] Alajmi, B., 2013. Design and control of photovoltaic systems in distributed generation. PhD. thesis, University of Strathclyde.

[27] Design of a DC-DC Converter for Photovoltaic Solar system. Available: https://sci hub.se/10.1109/iicpe.2012.6450508

[28] K.Rahrah. 2015. Photovoltaic pumping system in Bejaia climate with battery storage.

[29] M.tech scholars and al. Grid Connected Photovoltaic Power Plant with DC Boost converter Using MPPT Technique, International Research Journal of Engineering and Technology (IRJET), Volume: 04 Issue: 02 | Feb -2017.

[30] M.S.Sivagamasundari and al. Maximum Power Point Tracking For Photovoltaic System by Perturb and Observe Method Using Buck Boost Converter, International Journal of Advanced Research in Electrical, Electronics and Instrumentation Engineering, Vol. 2, Issue 6, June 2013.

[31] Adam TOMASZUK, Adam KRUPA. Step-up DC/DC converters for photovoltaic applications - theory and performance, PRZEGLĄD ELEKTROTECHNICZNY, R. 89 NR 9/2013

[32] : Brian T. Lynch .Under the Hood of a DC/DC Boost Converter.

[33] : M. H. Rashid, M. H. Rashid, and M. H. Rashid, Power electronics: circuits, devices, and applications, vol. 2. Prentice hall NJ, 1988.

[34] : Byoung-Kuk Lee, and Mehrdad Ehsani. A Simplified Functional Simulation Model for Three-Phase Voltage-Source Inverter Using Switching Function Concept . IEEE TRANSACTIONS ON INDUSTRIAL ELECTRONICS, VOL. 48, NO. 2, APRIL 2001.

[35] : Dr. D. Y. Patil , Saurabh Kharjule . Voltage Source Inverter International Conference on Energy Systems and Applications (ICESA) Institute of Engineering and Technology, Pune, India 30 Oct - 01 Nov, 2015

[36] : Balogh Tibor, Viliam Fedák, František Ďurovský. Modeling and Simulation of the BLDC Motor in MATLAB GUI ; Dept. of Electrical Engineering and Mechatronics, FEI TU of Košice, Slovak Republic. 978-1-4244-9312-8/11/ ©2011 IEEE

[37] : Padmaraja Yedamale, “Brushless DC (BLDC) Motor Fundamentals”, *Microchip Technology Inc., 2003.*

[38] : Rajan Kumar, Member, IEEE, and Bhim Singh, Fellow, IEEE ; Single Stage Solar PV Fed Brushless DC Motor Driven Water Pump . JESTPE-2016-12-0617.R2.

[39] Mohtar.A, Nedic.Z and Machotka.J (2008). Compact and Affordable BLDC Motor Controller for a Microelectronics Remote Laboratory.

[40] Gideon V. Leandro, Pedro A P Borges, Fabiano Salvadori, Mauricio Campos . Optimal Mathematical Model of Hall-effect Sensor, January 2008

[41] ''Hall effect and sensing'' Available : sensing.honeywell.com

[42] Alexandra Paun , Jean-Michel Sallese and Maher Kayal. Hall Effect Sensors Design , Integration and Behavior Analysis. Journal of Sensor and Actuator Networks 2013.

[43] Popovic, R.S. Hall Effect Devices, 2nd ed.; Institute of Physics Publishing: Bristol, UK, 2004.

[44] Salim Djeriou1, Aissa Kheldoun1 and Adel Mellit. Efficiency Improvement in Induction Motor-Driven SolarWate Pumping System Using Golden Section Search Algorithm.

[45] A.Moubarak. Variable Speed Photovoltaic Water Pumping Using Affinity Laws Article *in* Journal of Power and Energy Engineering . November 2017.

[46] Comparison of Different MPPT Algorithms with a Proposed One Using a Power Estimator for Grid Connected PV Systems. Hindawi Publishing Corporation International Journal of Photoenergy Volume 2016, Article ID 1728398, 10 pages. Available http://dx.doi.org/10.1155/2016/1728398

[47] Bedong, Kedah, Pratap Nair, Umayal . A Review on Photo Voltaic MPPT Algorithms Saravana Selvan. Faculty of Engineering and Computer Technology, AIMST University, Malaysia. International Journal of Electrical and Computer Engineering (IJECE) Vol. 6, No. 2, April 2016, pp. 567~582

[48] B. Kirisa;, O. Bingölb, R. Senolc and A. Altintasd , Solar Array System Layout Optimization for Reducing Partial Shading Effect. Vol. 130 (2016)

[49] Djalab, A., Bessous, N.,Rezaoui, M., & Merzouk, I.(2018). Study of the Effects of Partial Shading on PV array. Communication and Electrical Engineering. EL Oued,Algeria.

[50] Seyedmahmoudian,TM.,Mekhilef,S.,Rahmani,R.,Yusod,R.,& Renani,E.(2013).Analytical Modeling of partially Shaded Photovoltaic Systems.enrgies, 128-144.

[51] Bypass diodes in Solar Panels.(s.d).Electronics tutorials : https://www.electronics-tutorials.ws/diode/bypass-diodes.html

[52] Jirada Gosumbonggot and Goro Fujita. Partial Shading Detection and Global Maximum Power Point Tracking Algorithm for Photovoltaic with the Variation of Irradiation and Temperature. Graduate School of Engineering and Science, Shibaura Institute of Technology, Tokyo 135-8548, Japan;(2019)

[53] A MPPT Algorithm based on PSO for PV Array Under Partially Shaded Condition . Guihua Liu1*, Jianing Zhu1, Hailiang Tao1, Wei Wang1*, Frede Blaabjerg2 1School of Electrical Engineering and Automation, Harbin Institute of Technology, China. 2019 22nd International Conference on Electrical Machines and Systems (ICEMS).

[54] Ze,C .,Hang,Z.,& Hongzhi, Y.(2010). Research on MPPT control of PV system based on PSO algorithm . Chineese control and decision conference,(pp.887-892).Xuzhou, China.

[55] Wang Y , Bian N. (2015).Research of MPPT Control Method Based on PSO Algorithm. Computer Science and Network Technology ,(pp.698-701).Harbin,China.

[56] Jamaludin Mohamad Yatim , Azlan Mohd Zain and Nor Erne Nazira Bazin. Cuckoo Search Algorithm for Optimization Problems—A Literature Review and its Applications. Article *in* Applied Artificial Intelligence · May 2014 DOI: 10.1080/08839514.2014.90459.

[57] Ali M. Eltamaly . An Improved Cuckoo Search Algorithm for Maximum Power Point Tracking of Photovoltaic Systems under Partial Shading Conditions. Article *in* Energies · February 2021.

[58] Pierre Barthelemy, Jacopo Bertolotti, Diederik S Wiersma. A Levy flight for light. 2008 May, DOI: 10.1038/nature06948.

[59] A Maximum Power Point Tracking (MPPT) for PV system using Cuckoo Search with partial shading capability . Jubaer Ahmed, Zainal Salam . Centre for Electrical Energy Systems, Faculty of Electrical Engineering, Universiti Teknologi Malaysia, 81310 Johor Bahru, Malaysia. Applied Energy 119 (2014) 118–130

[60] P.C. Sen. Principles of Electric Machines and Power Electronics. John Wiley and Sons,1997.

[61] BLDC Motor Modelling and Control – A Matlab®/Simulink® Implementation – Master Thesis work by Stefán Baldursson –May, 2005

[62] PWM MANAGEMENT FOR 3-PHASE BLDC MOTOR DRIVES USING THE ST7MC.

[63] Position and Speed Control of Brushless DC Motors Using Sensorless Techniques and Application Trends, José Carlos Gamazo-Real, Ernesto Vázquez-Sánchez and Jaime Gómez-Gil

[64] Ward Brown. Brushless DC motor control made easy. Microchip technology INC,.2002

[65] Pawar.S.B,Kumbhar.N, & Diwan, S.P(2017). Single ended primary inductance converter based control BLDC motor drive. 2017 international conference on intelligent Computing, Instrumentation andControl Technologies (ICICICT). DOI: 10.1109/icicit1.2017.8342704.

[66] International Journal of Innovative Research in Science, Engineering and Technology (A High Impact Factor, Monthly, Peer Reviewed Journal) Visit: www.ijirset.com Vol. 7, Issue 1, January 2018

[67] P. Thirusakthimurugan, P. Dananjayan,' A New Control Scheme for The Speed Control of MBLDC Motor Drive' 1-4244-0342- 1/06/$20.00 ©2006 IEEE

[68] R.Krishnan, "Electric Motor Drives Modeling, Analysis, and Control, Prentice-Hall International Inc.,New Jersey, 2001.

[69] Ahmad Faiz Noor Azam, Auzani Jidin, Nor Azazi Ngatiman, M.H Jopri, Mustafa Manap, Adeline Lukar Herlino, Nor Faezah Alias . Current Control of BLDC Drives for EV Application .76100 Durian Tunggal, Malacca, Malaysia

[70] J.E.MURALIDHAR , P.VARANASI, Professor.Torque Ripple Minimization & Closed Loop Speed Control of BLDC Motor with Hysteresis Current Controller